Hydrothermally synthesized oxalate and phenanthroline based ferrimagnetic one-dimensional spin chain molecular magnets [{Fe(Δ)Fe(Λ)}1−x{Cr(Δ)Cr(Λ)}x(ox)2(phen)2]n (x =0, 0.1 and 0....

ARTICLE *in* JOURNAL OF MATERIALS CHEMISTRY · AUGUST 2013

Impact Factor: 7.44 · DOI: 10.1039/C3TC31288G

5 AUTHORS, INCLUDING:

Pramod Bhatt
Bhabha Atomic Research Centre
67 PUBLICATIONS **189** CITATIONS
SEE PROFILE

Sher Singh Meena
Bhabha Atomic Research Centre
151 PUBLICATIONS **543** CITATIONS
SEE PROFILE

Mayuresh Mukadam
Bhabha Atomic Research Centre
63 PUBLICATIONS **514** CITATIONS
SEE PROFILE

S. M. Yusuf
Bhabha Atomic Research Centre
277 PUBLICATIONS **2,290** CITATIONS
SEE PROFILE

Journal of Materials Chemistry C

RSC Publishing

PAPER

View Article Online
View Journal | View Issue

Cite this: *J. Mater. Chem. C*, 2013, **1**, 6637

Hydrothermally synthesized oxalate and phenanthroline based ferrimagnetic one-dimensional spin chain molecular magnets $[\{Fe(\Delta)Fe(\Lambda)\}_{1-x}\{Cr(\Delta)Cr(\Lambda)\}_x(ox)_2(phen)_2]_n$ ($x = 0$, 0.1 and 0.5) with giant coercivity of 3.2 Tesla

Pramod Bhatt,* Nidhi Thakur,† Sher Singh Meena, M. D. Mukadam and S. M. Yusuf

Oxalate (ox) and phenanthroline (phen) ligands based one dimensional spin chain molecular magnets, $[\{Fe(\Delta)Fe(\Lambda)\}_{1-x}\{Cr(\Delta)Cr(\Lambda)\}_x(ox)_2(phen)_2]_n$ ($x = 0$, 0.1, and 0.5) have been designed, and synthesized using a hydrothermal synthesis method. The Rietveld refinement of the powder X-ray and neutron diffraction patterns at room temperature confirms the single-phase formation of the compounds in the monoclinic structure with a space group $P2_1$. The compounds consist of two ligands, the oxalate ($C_2O_4^{2-}$) as a coordination acceptor building block and the neutral phen ($C_{12}H_8N_2$) as a coordination donor building block. Both ligands are connected to Fe ions of different symmetry {Fe(Δ) and Fe(Λ)}, thus forming an alternating zigzag chain like crystal structure having the repeating unit of [phen-Fe(Δ)-C_2O_4-Fe(Λ)-phen]$_n$. The chain is infinite in length and lies in the crystallographic *ac* plane. The interchain is well separated with an intermetallic distance of ~8.8 Å and the absence of an interchain π–π overlap between the organic ligands, resulting in a magnetic isolation between the interchains. The Mössbauer spectroscopy reveals the presence of high spin states of the Fe^{2+} ions of the compound for $x = 0$ whereas, both high-spin Fe^{2+} ($t_{2g}^4e_g^2$, $S = 2$) as well as low spin Fe^{2+} ($t_{2g}^6e_g^0$, $S = 0$) states are present for the compounds $x = 0.1$ and 0.5. The *dc* magnetization measurements show that the compounds exhibit spontaneous magnetization below ~9 K. The transition temperature is found to be ~8.7, 8.2 and 4.0 K for $x = 0$, 0.1 and 0.5 compounds, respectively. Moreover, a short range antiferromagnetic spin–spin correlation around 18–45 K has been observed for the compounds $x = 0$ and 0.1. An application of the Ising chain model to the *dc* magnetization data reveals the presence of a one-dimensional magnetic nature of all compounds with alternately spaced magnetic Fe sites. It is observed that the different Landé *g* factors (3.4 and 2.8) and exchange coupling constant values (−86 and −54 K) for $x = 0$ at two alternating Fe sites give rise to a ferrimagnetic-like behavior of the chains. The ferrimagnetic chain like structure transforms toward antiferromagnetic with Cr doping *i.e.* for $x = 0.1$ and 0.5. A hysteresis loop with a giant coercivity (3.2 T for $x = 0$) has been observed at 1.6 K, indicating a hard magnet-type behavior. The frequency dependence of the peak temperature in *ac* susceptibility *vs.* temperature curves for the $x = 0$ compound has been fitted and analyzed using the Arrhenius law as well as the power law, which exclude the possibility of a spin glass behavior. The fitted parameters ($\Delta/k_B = 208$ K and $\tau_0 = 2.9 \times 10^{-14}$ s obtained from the Arrhenius law, and $\tau_0 = 6.1 \times 10^{-8}$ s, and $z\nu = 2.6$ from the power law) show that the compound obeys the Glauber dynamics and is a real ferrimagnetic one-dimensional single chain magnet. In addition, the high pressure magnetization measurements for the $x = 0$ compound show an enhancement in the transition temperature from ~8.7 to 10.7 K with increasing pressure. The observation of both a one-dimensional spin chain nature and giant coercivity (3.2 Tesla) in such compounds opens up new opportunities to design and develop low dimensional molecular chain magnets through the appropriate choice of ligands using the hydrothermal synthesis method, because the observation of magnetic hysteresis of molecular origin in single-molecule magnets is considered one of the most relevant achievements in molecular magnetism.

Received 5th July 2013
Accepted 14th August 2013

DOI: 10.1039/c3tc31288g

www.rsc.org/MaterialsC

Solid State Physics Division, Bhabha Atomic Research Centre, Mumbai 400 085, India. E-mail: prabhatt@barc.gov.in; Fax: +91 22 25505151

† Present address: Department of Energy and Hydrocarbon Chemistry, Graduate School of Engineering, Kyoto University, Kyoto, Japan.

Introduction

Molecule-based magnets in which molecules, ions or ligands act as a building block are a new type of magnetic material. The

design and development of such molecule-based magnetic materials with multifunctional properties are the primary interest of the rapidly expanding research field of molecular magnetism.[1–3] The molecular magnets are suitable for their possible applications in the electronic and magnetic devices, electromagnetic shielding and information storage.[4–9] The advantages of molecule-based magnets over conventional magnets are their lightness, flexibility, solubility, biocompatibility, structural diversification, and easy processing ability at relatively lower temperatures. In addition, the physical properties of molecular magnets can be tailored by modifying the ligand field symmetry in organic synthetic chemistry.[10–14] However, despite their interesting physical properties and applications, the controlled synthesis and spontaneous generation of well-defined architectures (using both organic and inorganic building blocks) remains challenging. This is because the overall topology of the architectures is strongly influenced by the match (or mismatch) of a coordination algorithm of the linking metal ions with the binding properties (electronic, spatial, *etc.*) of the bridging ligands. Nevertheless, molecular architectures of bimetallic phases with a variety of extended networks have been synthesized using a multiple (one to three) choice of ligands with different transition metal ions. The discovery (at the beginning of the nineties) of such new polymeric bimetallic phases of variable dimensionality led to a great interest in the field of molecular magnetism.[15] In this regard, from the structural point of view, various types of architectures, which include one-dimensional (1D) chains, two-dimensional (2D) layers, and three-dimensional (3D) networks have been synthesized by incorporating oxalate ligands.[16–18] Since then, the oxalate ligand has been widely used for interconnecting different spin-bearing paramagnetic metal ions in extended networks due to its bis-chelating and coordinating ability and its remarkable capability to transmit electronic effects when acting as a bridge between two paramagnetic centers. Moreover, the oxalate ligand is as an excellent bridging ligand in supporting the magnetic exchange interaction (inter or intra) because of its smaller length of ~1–2 Å, which enhances the magnetic exchange interaction and Curie temperature strongly. In addition, the symmetry and anti-symmetry of the oxalate plays an important role in synthesizing new types of molecular magnets. Therefore, the fabrication of oxalate ligand based molecular magnets has attracted a great attention recently.[19–23] The well studied oxalate ligand based molecular magnets are denoted by $A[M^{II}M^{III}(ox)_n]$, {where M^{II} = Mn, Fe, Co, Cr, Ni, Cu; M^{III} = Cr, Fe; ox = oxalate and A is an organic or organometallic cation} which forms 2-D structures and behaves as ferro, ferri or canted antiferro-magnets with critical temperatures ranging from 5 to 44 K.[24–26] Similarly, the synthesis of bi-metallic infinite 2-or 3-D arrays on oxalate ligands has also been reported.[17,24,27–29] In this case, the magnetic exchange interaction between two different metal ions may be ferro- or antiferromagnetic, depending upon their respective electron configurations in conformity with the Kanamori–Goodenough rules.[30] Analogous to 3-D and 2-D magnets, there are reports on the synthesis of layered or 1-D chain magnets of oxalate ligands, which are magnetically isolated chains with a finite magnetization even in the absence of an applied magnetic field.[20,31,32] After the discovery of the first single-chain magnet (SCM)[33] $[Co^{II}(hfac)_2(NITPhOMe)]$, (hfac = hexafluoroacetylacetone, NITPhOMe = 4′-methoxyphenyl-4,4,5,5-tetramethylimidazoline-1-oxyl-3-oxide) by Gatteschi in 2001, there has been an increasing attraction towards the design of SCMs.[34–39] However, much attention has been paid to the SCMs based on bimetallic oxalate bridged phases incorporating π functional organic molecules.[40–42] In addition, the spontaneous magnetization, which is a rather rare phenomenon in the series of π-functional magnetic materials is also a current research of interest in SCMs.[43] Moreover, the π–π interaction, mainly responsible for tuning magnetic interaction between the metal centers may result in interesting physical properties.[44] Therefore, bridging between the metal centers through a π–π stacking may lead to a ferromagnetic or antiferromagnetic magnetic ordering with an enhanced magnetism by manipulating the metal ions, ligands, bridging angles, and interaction between the spin densities of the stacked layers. In this regard, the Ishii *et al.* have synthesized a 1-D cobalt radical coordination magnet with a huge coercivity, by introducing interchain interaction to the SCM system.[45] In addition, the oxalate and phenanthroline based π–π molecular magnets have also been recently synthesized which exhibit a spontaneous magnetization below 10 K.[43] Similarly, room temperature spontaneous magnetization in a coordination π–π framework has been reported.[44] It is believed that the incorporation of π molecule is expected to allow π–π interactions among these molecules, which may give rise to a short-range or a long-range magnetic ordering and consequently, emerging new materials with distinct magnetic properties. However, it is often found that the magnetic properties not only depend on the exchange coupling through the covalently bonded bridges but can also be strongly influenced by an intermolecular or an intramolecular interaction. In general, two types of interactions play an important role in determining the magnetic properties of chain magnets: (i) a hydrogen bonding interaction[46] and (ii) a π–π stacking interaction.[43] These interactions and hence the magnetic properties can be tailored by adding one or more inorganic paramagnetic ions at the lattice of the metallic ions. It is expected that by adding a new inorganic metallic centre, one could create new hybrid molecular materials with interesting properties or combinations of properties, depending on the nature of the cation and the possible interactions with the magnetic network. Thus, we synthesized oxalate and π functional (phenanthroline) ligand based molecular magnets $[\{Fe(\Delta)Fe(\Lambda)\}_{1-x}\{Cr(\Delta)Cr(\Lambda)\}_x(ox)_2(phen)_2]_n$ (x = 0, 0.1, and 0.5) using the hydrothermal synthesis method, and investigated their structural and magnetic properties. The X-ray and neutron diffraction studies confirm that such molecular magnets are one-dimensional (1-D) chains in nature that comprise alternating Fe(Δ) and Fe(Λ) assembled building units. In addition, the corresponding *ac* susceptibility, *dc* magnetization measurements, and the Ising theory with two different Landé *g* factors confirm the existence of the 1-D ferrimagnetic nature of the compound. In addition, an enhancement in the transition temperature with high pressure, the observation of giant coercivity and spontaneous

magnetization below 9 K has been observed in the compound. This oxalate and phenanthroline ligands based 1-D spin chain molecule magnet can be regarded as one of the hardest magnets with a giant coercivity of 3.2 Tesla.

Experimental

The compounds $[\{Fe(\Delta)Fe(\Lambda)\}_{1-x}\{Cr(\Delta)Cr(\Lambda)\}_x(ox)_2(phen)_2]_n$ with $x = 0$, 0.1, 0.5, and 1 were synthesized using a hydrothermal synthesis method. In the hydrothermal method, a heterogeneous reaction takes places in the presence of aqueous solvents under high pressure and temperature conditions to dissolve and recrystallize materials that are relatively insoluble under ordinary conditions. For the synthesis, we have adapted a procedure similar to that reported by Li *et al.*[43] with minor modifications. All the chemicals were of reagent grade, and used as received from Sigma-Aldrich. The hydrothermal reaction was carried out in a 250 mL Teflon-lined vessel at 190 °C in water. For the $x = 0$ compound, a reaction mixture of $FeCl_2 \cdot 4H_2O$ (0.796 g, 0.2 mmol), oxalic acid (0.756 g, 0.3 mmol), 1,10-phenanthroline monohydrate (0.792 g, 0.2 mmol), H_2O (160 mL, 440 mol) in molar ratios of 2 : 3 : 2 : 4400 and 4 mL CsOH were sealed in a 250 mL Teflon-lined stainless-steel autoclave, heated to 190 °C within 3 h at a rate of ~60°C h^{-1}, kept at 190 °C for 96 h, cooled to 70 °C at a rate of 6°C h^{-1}, and then left to cool to room temperature. The above mentioned procedure was followed for the $x = 0.1$ compound, {materials used were $CrCl_2$ (0.049 g, 0.2 mmol) and $FeCl_2 \cdot 4H_2O$ (0.716 g, 0.2 mmol)}, $x = 0.5$ {$CrCl_2$ (0.122 g, 0.2 mmol) and $FeCl_2 \cdot 4H_2O$ (0.398 g, 0.2 mmol)} and for the compound with $x = 1$, {$CrCl_2$ (0.245 g, 0.2 mmol)}. The precipitate was filtered, and washed many times with EtOH and finally allowed to dry in the air. This synthesis was reproducible and the yield of the compounds was calculated and found to be 35% which are based on the concentration of $FeCl_2$ and $CrCl_2$. The values obtained from elemental analysis in wt% are summarized here: for $x = 0$, formula $Fe_2C_{28}H_{16}N_4O_8$, calculated Fe: 17.2, C: 51.9, H: 2.5, N: 8.6; and found Fe: 17.3, C: 52.1, H: 3.2, N: 8.8. For $x = 0.1$, formula $Fe_{1.8}Cr_{0.2}C_{28}H_{16}N_4O_8$, calculated Fe: 15.2, Cr: 1.6; and found Fe: 15.8, Cr: 1.2. For $x = 0.5$, formula $Fe_1Cr_1C_{28}H_{16}N_4O_8$, calculated Fe: 8.6, Cr: 8.0; and found Fe: 9.1, Cr: 8.1.

The X-ray diffraction (XRD) measurements of all the compounds were performed at room temperature in a Bragg–Brentano geometry using a Rigaku diffractometer over an angular (2θ) range of 10–70° in equal 2θ steps of 0.02° using Cu K_α radiation. A detailed structural analysis was performed on the XRD data by the Rietveld refinement method with the FullProf program.[47]

The neutron diffraction patterns for the $x = 0$ and $x = 0.1$ compounds were recorded using the wavelength, $\lambda = 1.249$ Å at 300 K on the five linear position-sensitive detectors (PSD) based powder diffractometer-II at the Dhruva reactor, Trombay, India.

Mössbauer spectra were recorded for the $[\{Fe(\Delta)Fe(\Lambda)\}_{1-x}\{Cr(\Delta)Cr(\Lambda)\}_x(ox)_2(phen)_2]_n$ with $x = 0$, 0.1 and 0.5 samples using a Mössbauer spectrometer (Nucleonix Systems Pvt. Ltd., Hyderabad, India) operated in the constant acceleration mode (triangular wave) in a transmission geometry at room temperature. The source employed was Co-57 in a Rh matrix of strength 50 mCi. The calibration of the velocity scale was done by using an enriched α-^{57}Fe metal foil. The line width (inner) of the calibration spectrum was 0.23 mm s^{-1}.

The magnetization measurements were carried out using a Cryogenic Ltd., UK made commercial physical properties measurements system as a function of both the temperature and magnetic field. The temperature dependent magnetization measurements were carried out in zero-field-cooled (ZFC) and field-cooled (FC) conditions down to 5 K. For the ZFC measurements, the sample was cooled from room temperature down to the lowest temperature in the absence of a magnetic field, and the magnetization was measured in the warming cycle with the applied magnetic field on. Whereas in the FC measurements, the sample was cooled from room temperature down to the lowest temperature in the presence of applied magnetic field and the magnetization was measured in the warming cycle under the same field. Hysteresis curves were recorded at 5 K and 1.8 K over a +90 to −90 kOe applied magnetic field for $[\{Fe(\Delta)Fe(\Lambda)\}_{1-x}\{Cr(\Delta)Cr(\Lambda)\}_x(ox)_2(phen)_2]_n$ with the $x = 0$, 0.1, and 0.5 compounds.

The magnetization measurements under high pressure were carried out in the physical properties measurements system using a commercially available pressure cell (Mcell 10 module) from EasyLab, UK. The sample was first placed in a Teflon cell with coal oil as the pressure media. Then the Teflon cell (EasyLab, UK) was set in a copper–beryllium pressure cell for the magnetization measurement. A maximum pressure of 0.8 GPa, determined using Sn as an internal manometer was used for the present study.

The measurements of the temperature dependence of the *ac* magnetic susceptibility in the range 7–10 K were carried out at various frequencies between 20 Hz and 10 kHz using a commercial *ac* susceptibility probe (Cryogenic Ltd., UK) with an *ac* field of 5 Oe.

Results and discussion

(A) X-ray and neutron diffraction study

Both X-ray and neutron powder diffraction measurements at room temperature were used for the structural characterization of the compounds. Fig. 1 presents the Rietveld refined (using the FullProf program)[47] room temperature X-ray {Fig. 1(a)} and neutron powder diffraction patterns {Fig. 1(b)} of the $[\{Fe(\Delta)Fe(\Lambda)\}_{1-x}\{Cr(\Delta)Cr(\Lambda)\}_x(ox)_2(phen)_2]_n$ compounds. It is evident from the fitted XRD and neutron diffraction patterns that the compounds where $x = 0$ and 0.1, 0.5 are in a single crystalline phase. The crystal structure of the compounds ($x = 0$, 0.1, and 0.5) is indexed with a monoclinic structure of the space group $P2_1$. Whereas, for $x = 1$, the compound is in mixed phases consisting of (i) a monoclinic structure with the space group $P2_1$ and (ii) an impurity phase (due to formation of nanoparticles of chromium oxides). The formation of nanoparticles of chromium oxides using the hydrothermal method has been reported in the literature and supports our observation.[48] Therefore, we are not discussing the properties of the compound where $x = 1$ further due to the formation of an impurity phase. The important structural parameters, such as the atomic coordinates, lattice constant,

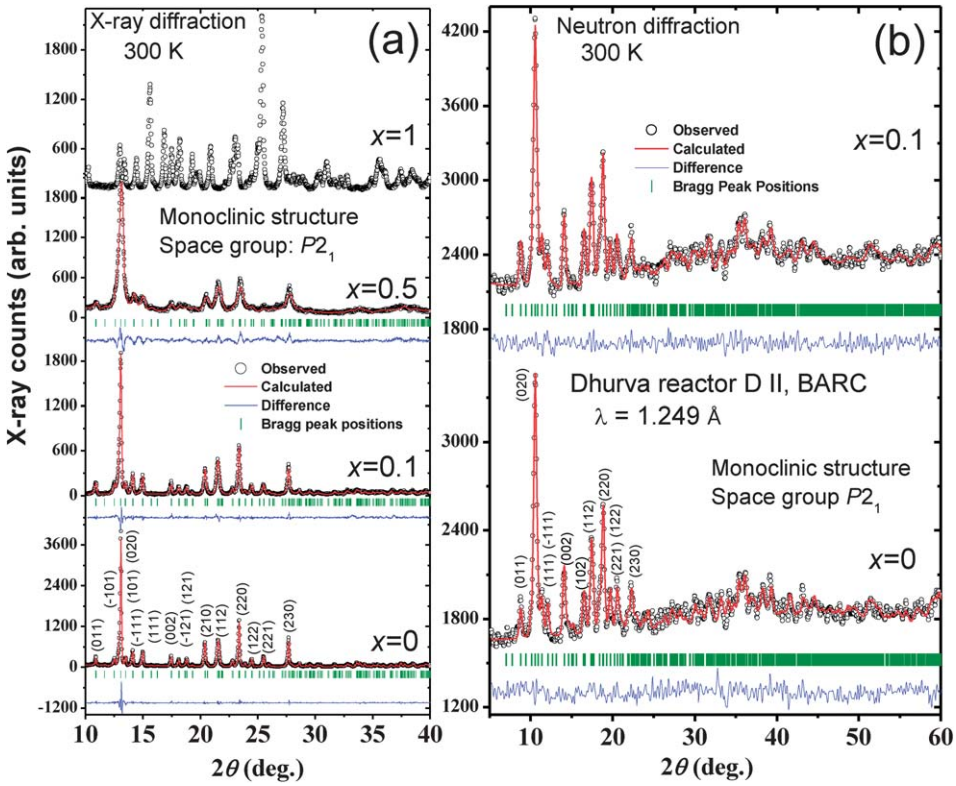

Fig. 1 Rietveld refined room temperature XRD (a) and neutron diffraction (b) patterns of $[\{Fe(\Delta)Fe(\Lambda)\}_{1-x}\{Cr(\Delta)Cr(\Lambda)\}_x(ox)_2(phen)_2]_n$ compounds for $x = 0$, 0.1, 0.5 and 1.0. Open circles and solid lines indicate the observed and the calculated patterns, respectively. Solid lines at the bottom show the difference between the observed and calculated patterns. Vertical lines at the bottom of XRD patterns show the position of the allowed Bragg peaks. The (*hkl*) values of the corresponding Bragg peaks are also marked for the compounds. The structures are indexed and fitted with a monoclinic structure of space group $P2_1$.

bond length, bond angles and site occupancies, derived from the Rietveld analysis of the X-ray diffraction, are shown in Table 1 for the compounds with $x = 0$, 0.1, and 0.5. The room temperature neutron diffraction patterns (recorded at 1.249 Å wavelength) are also consistent with the results derived from the X-ray diffraction patterns for these compounds. The X-ray and neutron diffraction studies reveal that the Cr^{2+} ions also resides at the same crystallographic position of the Fe^{2+} (2*a*) for the compound with $x = 0.1$ and 0.5. The composition dependence of the lattice constants and bond angles for $x = 0$, 0.1 and 0.5 compounds, derived from the Rietveld refinement XRD patterns are shown in Fig. 2. It is interesting to see that the lattice constants slightly change with Cr^{2+} doping, particularly in *c*. However, a considerable change has been observed in the bond angle (β) with Cr doping. This change in bond angle suggests that the lattice distortion appears in the compound with increasing Cr^{2+} concentrations.

In order to elucidate further the crystal structure of the compound in more detail, we have shown the crystallographic atomic positions (obtained from the Rietveld refined XRD patterns) of the compound in Fig. 3. A chain like structure of the compound was observed. The single repeating unit of the chain is shown in Fig. 3(a). It is seen that two crystallographically distinct Fe^{2+} ions $\{Fe(\Delta) = Fe_1$ and $Fe(\Lambda) = Fe_2\}$ are bridged by the oxalate ligand *i.e.* four oxygen atoms of the oxalate ion. Both the Fe^{2+} ions are separated from each other with an intermetallic distance of ~5.51 Å.

Moreover, both the Fe^{2+} ions {Fe(Δ) and Fe(Λ)} are also connected with two nitrogen atoms of the phen group. Though the Fe(Δ) and Fe(Λ) are connected with similar atoms at both sites, they are different in terms of their bond lengths and bond angles with respect to each other (see Table 1). Therefore, both the Fe ions are slightly asymmetric in nature. Such arrangements of these two locally distinct asymmetric Fe^{2+} ions {Fe(Δ) and Fe(Λ)} thus form chirality in the structure *i.e.* being the same attachments of two Fe^{2+} ions with other ions (such as O and N) they are not superimposable on the mirror image [Fig. 3(b)]. In addition, the symmetry of a molecule, which determines the chirality of both the Fe^{2+} ions {Fe(Δ) and Fe(Λ)} are different and therefore denoted as Fe(Δ) and Fe(Λ) respectively for Fe_1, and Fe_2 {Fig. 3(b)}. The distance between the C atoms between two phen ligands was found to be ~14.95 Å. The repetition of a single repeating unit results in an infinite 1-D zigzag chain like structure of the compound, as shown in Fig. 3(c). The chain of the type [phen-Fe(Δ)-C_2O_4-Fe(Λ)–phen] in which the phen ligands are bound to the Fe ions and the oxalate ligand bridges the metallic ions, lies in the crystallographic *ac* plane. The π–π interactions within the phen groups between the zigzag chains develop a quasi 2-D framework within the *ac* plane, and hence, the magnetic properties of the chain will be strongly correlated with the dimensionality, magnetic interactions, intra- and interchain distances. The chains are well separated with each other with an intermetallic

Table 1 Structural parameters of the Rietveld refined X-ray powder diffraction patterns of the $[\{Fe(\Delta)Fe(\Lambda)\}_{1-x}\{Cr(\Delta)Cr(\Lambda)\}_x(ox)_2(phen)_2]_n$ compounds. (x, y and z denote the fractional coordinates)

Compounds	Atom	x	y	z	Occupancy	Bond length (Å)	Bond Angles
$x = 0$	Fe_1	0.132(6)	0.969(6)	0.402(9)	1	Fe_1–O_1: 2.32(6)	O_1–Fe_1–O_2: 68.2(6)
$a = 9.233(8)$ Å	Fe_2	0.61(6)	0.978(3)	0.101(8)	1	Fe_1–O_2: 2.22(4)	O_1–Fe_1–N_2: 118(3)
$b = 13.545(9)$ Å	O_1	1.044(1)	0.228(2)	0.039(3)	1	Fe_1–O_6: 2.15(6)	O_1–Fe_1–O_6: 95.2(5)
$c = 10.295(6)$ Å	O_2	0.333(5)	0.891(9)	0.353(3)	1	Fe_1–O_8: 2.26(5)	O_1–Fe_1–O_8: 86.6(19)
$\alpha = \gamma = 90$	O_3	0.499(2)	0.893(7)	0.234(5)	1	Fe_1–N_1: 2.28(5)	O_1–Fe_1–N_1: 162 (3)
$\beta = 94.36(6)$	O_4	0.421(2)	1.069(4)	0.144(3)	1	Fe_1–N_2: 2.84(6)	
$V = 1283.7$ (Å)^3	O_5	0.814(1)	0.894(4)	0.127(1)	1		
	O_6	−0.066(8)	1.052(1)	0.378(8)	1	Fe_2–O_3: 2.13(1)	O_4–Fe_2–O_3: 78.1(6)
$C_{28}H_{16}Fe_2N_4O_8$	O_7	0.732(3)	1.050(7)	0.286(5)	1	Fe_2–O_4: 2.25(3)	O_4–Fe_2–N_4: 111(3)
MW = 647.68	O_8	0.032(7)	0.861(3)	0.254(4)	1	Fe_2–O_5: 2.14(6)	O_4–Fe_2–O_5: 161.9(8)
	N_1	0.092(4)	0.866(2)	0.572(1)	1	Fe_2–O_7: 2.32(5)	O_4–Fe_2–O_7: 86.2(17)
	N_2	0.183(9)	1.054(1)	0.657(3)	1	Fe_2–N_3: 2.41(6)	O_4–Fe_2–N_3: 107 (3)
	N_3	0.721(2)	1.05485	−0.082(1)	1	Fe_2–N_4: 2.51(6)	
	N_4	0.551(9)	0.848(7)	−0.068(7)	1		
$x = 0.1$	Fe_1	0.129(9)	0.965(1)	0.398(7)	0.9	Fe_1–O_1: 2.10(2)	O_1–Fe_1–O_2: 72.1(2)
$a = 9.216(5)$ Å	Fe_2	0.618(5)	0.973(5)	0.097 (6)	0.9	Fe_1–O_2: 1.81(6)	O_1–Fe_1–N_2: 99.3(2)
$b = 13.565(5)$ Å	Cr_1	0.129(9)	0.965(1)	0.398(7)	0.1	Fe_1–O_6: 2.04(5)	O_1–Fe_1–O_6: 90.1(12)
$c = 10.201(6)$ Å	Cr_2	0.618(5)	0.973(5)	0.097 (6)	0.1	Fe_1–O_8: 2.16(2)	O_1–Fe_1–O_8: 91.4(12)
$\alpha = \gamma = 90$	O_1	0.205(6)	1.032 (4)	0.239(2)	1	Fe_1–N_1: 2.08(8)	O_1–Fe_1–N_1: 172.1(3)
$\beta = 94.291(6)$	O_2	0.301(7)	0.908(5)	0.365(6)	1	Fe_1–N_2: 2.04(6)	
$V = 1271.7$ (Å)^3	O_3	0.482(6)	0.891(4)	0.208(5)	1		
	O_4	0.409(8)	1.064(5)	0.140(8)	1	Fe_2–O_3: 2.06(9)	O_4–Fe_2–O_3: 69.0(5)
$C_{28}H_{16}Fe_{1.8}Cr_{0.2}N_4O_8$	O_5	0.807(5)	0.902(4)	0.105(5)	1	Fe_2–O_4: 2.35(6)	O_4–Fe_2–N_4: 105.3(2)
MW = 646.9	O_6	−0.067(8)	1.034(5)	0.365(8)	1	Fe_2–O_5: 1.98(4)	O_4–Fe_2–O_5: 167.1(2)
	O_7	0.702(7)	1.047(5)	0.238(8)	1	Fe_2–O_7: 1.86(2)	O_4–Fe_2–O_7: 83.0(8)
	O_8	−0.035(8)	0.886(6)	0.279(8)	1	Fe_2–N_3: 2.59(6)	O_4–Fe_2–N_3: 95.8(12)
	N_1	0.079(8)	0.906(6)	0.578(7)	1	Fe_2–N_4: 2.34(7)	
	N_2	0.218(8)	1.058(6)	0.541(9)	1		
	N_3	0.715(8)	1.091(6)	−0.027(8)	1		
	N_4	0.559(7)	0.890(7)	−0.101(7)	1		
$x = 0.5$	Fe_1	0.128(8)	0.964(7)	0.398(2)	0.5	Fe_1–O_1: 2.09(3)	O_1–Fe_1–O_2: 71.4(3)
$a = 9.17(8)$ Å	Fe_2	0.61(9)	0.973(7)	0.098(1)	0.5	Fe_1–O_2: 1.81(8)	O_1–Fe_1–N_2: 88.3(5)
$b = 13.55(5)$ Å	Cr_1	0.128(8)	0.964(7)	0.398(2)	0.5	Fe_1–O_6: 1.94(8)	O_1–Fe_1–O_6: 91.9(7)
$c = 10.20(6)$ Å	Cr_2	0.61(9)	0.973(7)	0.098(1)	0.5	Fe_1–O_8: 2.16(1)	O_1–Fe_1–O_8: 91.4(2)
$\alpha = \gamma = 90$	O_1	0.205(1)	1.034(4)	0.233(1)	1	Fe_1–N_1: 2.32(4)	O_1–Fe_1–N_1: 130.6(5)
$\beta = 93.79(6)$	O_2	0.301(4)	0.909(1)	0.363(8)	1	Fe_1–N_2: 2.69(8)	
$V = 1264.6$ (Å)^3	O_3	0.483(3)	0.890(9)	0.209(1)	1		
	O_4	0.410(5)	1.062(5)	0.1400	1	Fe_2–O_3: 2.06(3)	O_4–Fe_2–O_3: 69.8(8)
$C_{28}H_{16}Fe_1Cr_1N_4O_8$	O_5	0.807(3)	0.902(9)	0.102(7)	1	Fe_2–O_4: 2.32(1)	O_4–Fe_2–N_4: 88.5(7)
MW = 643.8	O_6	−0.063(7)	1.02(7)	0.367(7)	1	Fe_2–O_5: 1.98(8)	O_4–Fe_2–O_5: 168.0(3)
	O_7	0.703(5)	1.048(2)	0.240(8)	1	Fe_2–O_7: 1.89(7)	O_4–Fe_2–O_7: 83.1(8)
	O_8	−0.036(2)	0.886(9)	0.277(7)	1	Fe_2–N_3: 2.64(4)	O_4–Fe_2–N_3: 102.4(2)
	N_1	0.950(7)	1.025(5)	0.607(5)	1	Fe_2–N_4: 2.65(4)	
	N_2	0.298(6)	1.088(2)	0.550(7)	1		
	N_3	0.766(9)	1.10(2)	−0.037(2)	1		
	N_4	0.571(5)	1.018(4)	−0.153(3)	1		

distance {between Fe(Δ) = Fe_1 and Fe(Λ) = Fe_2} of ~8.8 Å suggesting a negligible interchain magnetic interaction. The distances between two nearest phen groups within the intrachain and interchain direction are found to be ~7.8 Å and 4.5 Å, respectively, which suggests the possibility of a weak π–π magnetic interaction along the interchain {Fig. 3(d) and (e)}.

As mentioned earlier, both the Fe(Δ) and Fe(Λ) ions in the chains (for $x = 0$) are asymmetric in nature with respect to each other. However, it is observed that, though the lattice constant and space group symmetry do not change significantly with Cr^{2+} doping, a decrease in the bond length and bond angle has been observed leading to a reduction in the cell volume (see Table 1). Moreover, the lattice distortion increases in the compound with increasing Cr^{2+} doping. Fig. 4(a) and (b) and shows the lattice distortion in the compound with $x = 0.1$ and $x = 0.5$, as compared to that for the $x = 0$. The Mössbauer spectroscopy study, which is discussed in the next section, also supports the finding that more lattice distortion occurs in the compound with an increasing Cr^{2+} doping.

(B) Mössbauer spectroscopy study

In order to confirm the Fe^{2+} ion's spin states and their local atomic surroundings, a room temperature Mössbauer

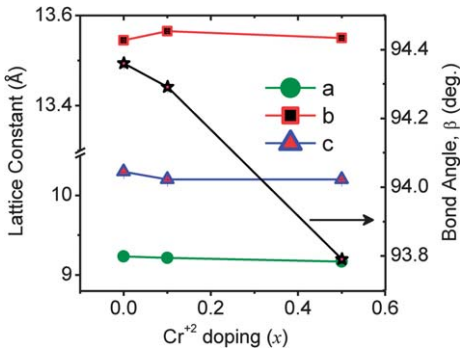

Fig. 2 Variation of lattice constants (left side) and β bond angle (right side) with Cr doping in $[\{Fe(\Delta)Fe(\Lambda)\}_{1-x}\{Cr(\Delta)Cr(\Lambda)\}_x(ox)_2(phen)_2]_n$ compounds.

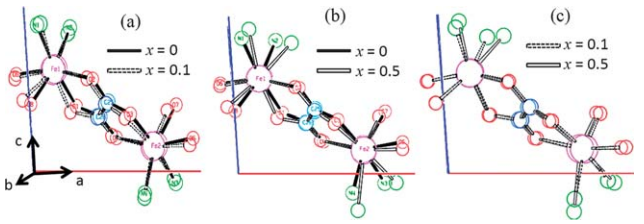

Fig. 4 Comparison of lattice distortion appears between two compounds with Cr^{2+} doping (a) $x = 0$ and $x = 0.1$, (b) $x = 0$ and $x = 0.5$, (c) $x = 0.1$ and $x = 0.5$.

spectroscopic study was carried out for the $x = 0$, 0.1, and 0.5 compounds. The hyperfine interaction around the Fe ions was analyzed from the fitted Mössbauer spectra, recorded at a velocity of $\pm$ 4.5 mm s^{-1}. A room temperature Mössbauer spectrum of $[\{Fe_1(\Delta)Fe_2(\Lambda)\}(ox)_2(phen)_2]_n$ for the $x = 0$ compound is shown in Fig. 5(a). No magnetic hyperfine pattern is observed in the Mössbauer spectrum (inset shows an absence of any six line hyperfine pattern at higher velocity, confirming its paramagnetic nature at room temperature). The fitting of the data indicates the presence of two symmetric paramagnetic doublets (A and B), suggesting that both the Fe ions {Fe(Δ) and Fe(Λ)} have different environments. The fitted Mössbauer parameters, such as the isomer shift (δ), quadrupole splitting (ΔE_Q), and line width (Γ) for all compounds ($x = 0$, 0.1, and 0.5) are listed in Table 2. The ΔE_Q values of the two doublets were found to be 1.757 and 1.822 mm s^{-1}, respectively. Both doublets (A and B) with high ΔE_Q values show an asymmetry around both the Fe ions, which is due to the monoclinic structure of the compound. The corresponding δ values were found to be 1.063 and 1.091 mm s^{-1}. The observed δ values indicate that both Fe^{2+} ions are in the high spin (HS) state.[49] The different δ and ΔE_Q values of both Fe ions in the compound can be understood from the structural point of view. From the crystal structure shown in Fig. 3, it may be noted that both the Fe^{2+} ions are surrounded by similar atoms (C, O and N), therefore both the Fe(Δ) and Fe(Λ) ions are in high spin states. However, they are different in terms of their bond length and bond angles resulting in a different asymmetry and different charge density on both the Fe ions in the compound. The areas under these two doublets A and B (Table 2) are found to be 53.7% and 46.3%, respectively. The identification of both the doublet for the Fe ions {Fe(Δ) and Fe(Λ)} was done on the basis of the δ values. The δ value for the doublet A is lower than the doublet B, indicating that the

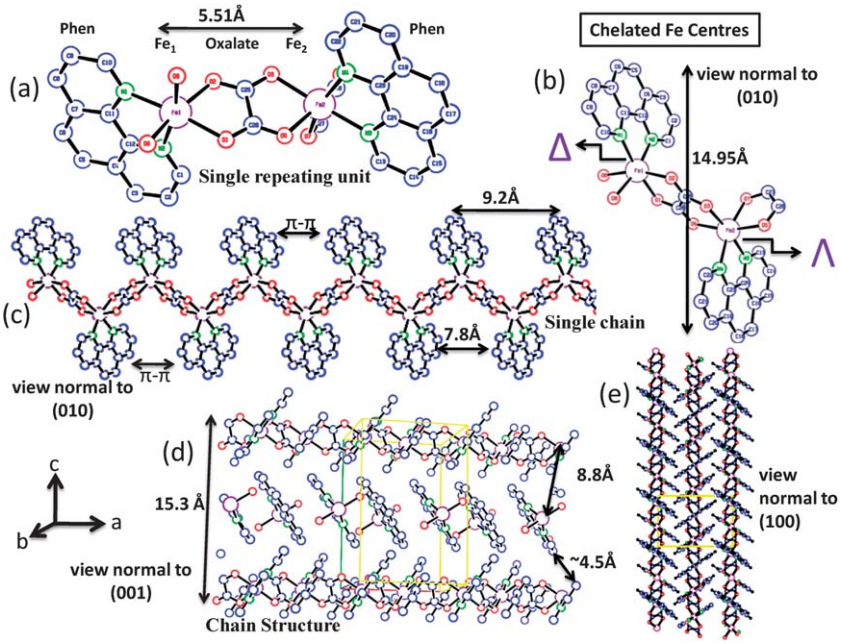

Fig. 3 Crystal structural of the $[\{Fe(\Delta)Fe(\Lambda)\}(ox)_2(phen)_2]_n$ compound. The repetition of the single repeating unit of the chain (a) with chelated Fe centers (b) results an infinite 1-D zigzag chain like structure (c) of the compound. One unit cell of the compound contains three intra-chains which are well separated from each other, as shown in two different directions (d) and (e). Color coding of the compound: Fe (magenta), N (green), C (blue), O (red). The H atoms are omitted for a better illustration. Symmetry for the monoclinic structure: (1) x, y, z (2) $-x, y + 1/2, -z$.

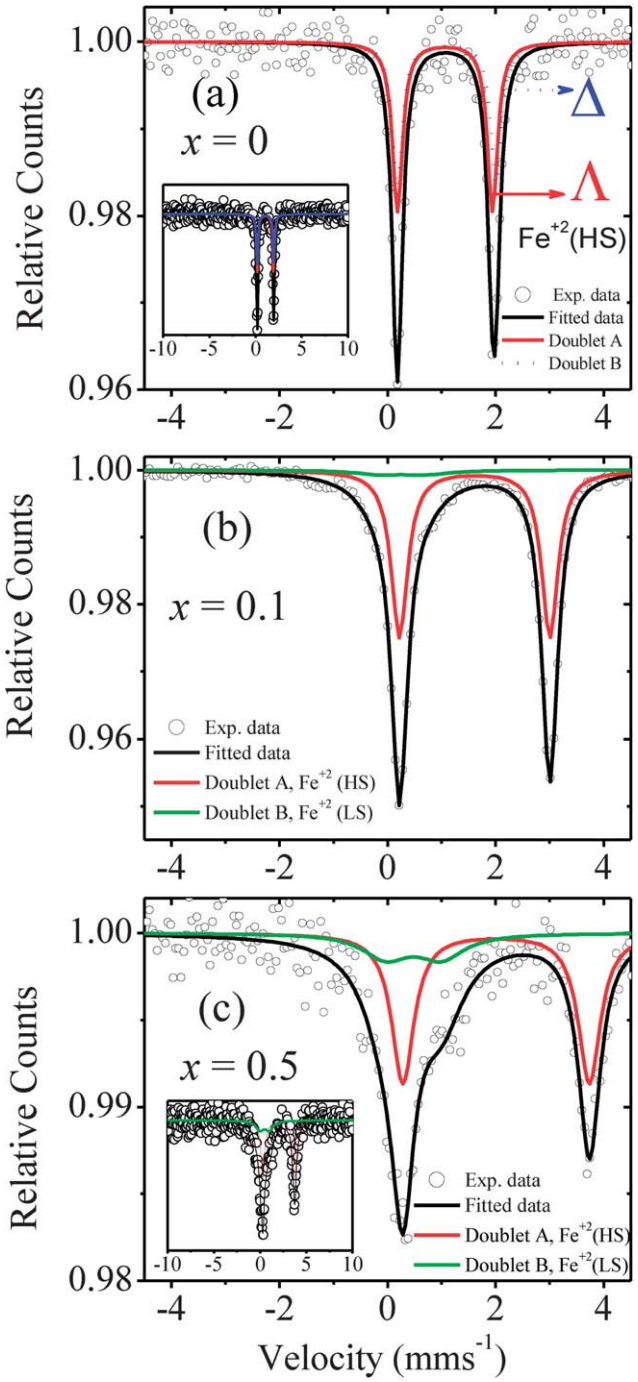

Fig. 5 Room temperature Mössbauer spectra of the $[\{Fe(\Delta)Fe(\Lambda)\}_{1-x}\{Cr(\Delta)Cr(\Lambda)\}_x(ox)_2(phen)_2]_n$ compounds with $x = 0$ (a), $x = 0.1$ (b), and $x = 0.5$ (c). The inset of (a) and (c) shows the absence of six line magnetic patterns, recorded at a higher velocity of ± 10 mm s^{-1}. Open circles show the experimental data and the thick solid line is the least square fitted curve.

charge density on this Fe ion is higher. It is also clear from our XRD analysis that the average bond length of Fe_1–O/N with its ligand ions is higher than the Fe_2–O/N ions. It means that the electronic charge density will be lower around the Fe(Δ) ions, resulting in the higher isomer shift value for the Fe(Δ) ion.[49–51] Thus, the doublet B belongs to the Fe(Δ) ion, and the doublet A belongs to the Fe(Λ) ions in the compound. In addition, the higher value of ΔE_Q for the doublet B indicates more distortion around the Fe(Δ) ions relative to the Fe(Λ) ions. The room temperature Mössbauer spectra of the compounds $[\{Fe(\Delta)Fe(\Lambda)\}_{1-x}\{Cr(\Delta)Cr(\Lambda)\}_x(ox)_2(phen)_2]_n$ with $x = 0.1$ and 0.5 are shown in Fig. 5(b) and (c), respectively. The Mössbauer spectra of both compounds are fitted with two symmetric doublets. The δ values of both the doublets for the $x = 0.1$ compound are found to be 1.614 (doublet A) and 0.258 mm s^{-1} (doublet B), respectively. The observed δ values indicate that the doublet A is due to a HS Fe^{2+} ions, and the doublet B belongs to a low spin (LS) Fe^{2+} ions. The areas under these two doublets A and B (Table 2) are found to be 84% (HS) and 16% (LS), respectively. Moreover, the ΔE_Q value for the HS Fe^{2+} ions in $x = 0.1$ is also found to increase when compared to that of the $x = 0$ compound, indicating more distortion of the high spin Fe^{2+} ions in the compound $x = 0.1$. Generally, the ΔE_Q values arise due to an interaction between the nuclear quadruple moment and the electric field gradient, produced by the surrounding ions (oxygen and nitrogen ions in the present case), the different values of ΔE_Q for the two compounds suggest a different local environment for the 2*a* sites of the Fe ions. The higher value of ΔE_Q for the compound $x = 0.1$ of doublet A as compared to that of the compound $x = 0$ (doublet A) indicates the presence of a relatively larger crystal field gradient at the Fe site resulting in more distortion. On further Cr^{2+} doping ($x = 0.5$ compound), the ΔE_Q values for doublet A and doublet B further increase (3.450 and 1.033 mm s^{-1}, respectively), suggesting that the distortion increases at both the HS and LS Fe^{2+} sites. Moreover, the relative area (41.1%) of the LS Fe^{2+} ions increases with Cr^{2+} doping. In conclusion, the Mössbauer results confirm that there are two atomic Fe^{2+} sites (both in the HS states) in the compound ($x = 0$) with nearly an equal relative area, whereas, on Cr^{2+} doping ($x = 0.1$ and 0.5 compounds), both the distortion and the LS states of the Fe^{2+} ions increase.

(C) *dc* magnetization study

The field-cooled (FC) and zero-field cooled (ZFC) magnetization *versus* temperature (T) curves under an external applied magnetic field of 50 and 100 Oe for $[\{Fe(\Delta)Fe(\Lambda)\}_{1-x}\{Cr(\Delta)Cr(\Lambda)\}_x(ox)_2(phen)_2]_n$ with $x = 0$ are shown in Fig. 6(a) and (b), respectively. The compound shows a magnetic transition below ~10 K. The magnetic transition seems to be ferromagnetic or ferrimagnetic in nature. In addition, a rapid rise below 10 K, a peak in the zero-field-cooled (ZFC) magnetization and saturation at the lower temperature in the field-cooled (FC) has been observed. However, with increasing magnetic field (100 Oe), a suppression of the peak in the zero-field-cooled (ZFC) magnetization indicates an antiferromagnetic ordering in nature, whereas the observation of saturation (also suppressed by the field) reflects a (weak) ferromagnetic-like-ordering of the compound.

A branching in the FC and ZFC magnetization curves has been observed for the compounds, which can be discussed in terms of the formation of magnetic domains and the domain wall motion under various cooling conditions.[52,53] In the ZFC

Table 2 Hyperfine parameters (extracted from the Mössbauer spectra) for the $[\{Fe(\Delta)Fe(\Lambda)\}_{1-x}\{Cr(\Delta)Cr(\Lambda)\}_x(ox)_2(phen)_2]_n$ compounds with $x = 0$, 0.1, and 0.5

Compound	Doublet	Spin state of Fe^{2+} ion	Quadrupole splitting (ΔE_Q) mm s^{-1}	Isomer shift (δ) mm s^{-1}	Line width (Γ) mm s^{-1}	Area R_A (%)
$x = 0$	A	HS	1.757 ± 0.010	1.063 ± 0.01	0.230 ± 0.01	53.7
	B	HS	1.822 ± 0.011	1.091 ± 0.01	0.230 ± 0.01	46.3
$x = 0.1$	A	HS	2.784 ± 0.02	1.614 ± 0.01	0.367 ± 0.03	84.0
	B	LS	0.852 ± 0.06	0.258 ± 0.03	1.037 ± 0.1	16.0
$x = 0.5$	A	HS	3.450 ± 0.02	1.920 ± 0.01	0.496 ± 0.03	58.9
	B	LS	1.033 ± 0.08	0.482 ± 0.04	1.038 ± 0.14	41.1

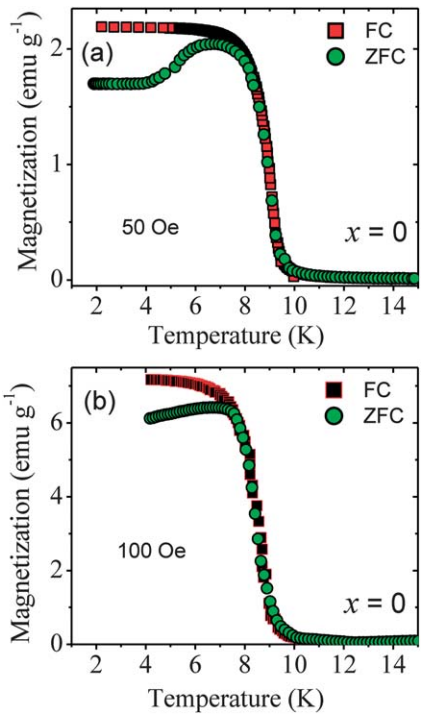

Fig. 6 The field-cooled (FC) and zero-field cooled (ZFC) magnetization *versus* temperature (T) curves under an external applied magnetic field of 50 (a) and 100 Oe (b) of the compound $[\{Fe(\Delta)Fe(\Lambda)\}_{1-x}\{Cr(\Delta)Cr(\Lambda)\}_x(ox)_2(phen)_2]_n$ for $x = 0$.

process, *i.e.* when the field is zero, the magnetic domains are randomly disordered in the compound at room temperature, showing a zero magnetization. When the sample is cooled in a field, the spin moments are ordered, and almost parallel to the direction of applied field. The cooling of the sample under a magnetic field would favor the growth of domains in the direction of the applied magnetic fields and hence it would result in a higher value of magnetization as compared to the ZFC magnetization.

Fig. 7 shows the FC magnetization *versus* T curves under an external applied magnetic field of 100 Oe for the compounds $[\{Fe(\Delta)Fe(\Lambda)\}_{1-x}\{Cr(\Delta)Cr(\Lambda)\}_x(ox)_2(phen)_2]_n$ with $x = 0$, 0.1, and 0.5. From this figure, it is clearly seen that both magnetization and transition temperature (observed ~8.7 K, for $x = 0$) for the compounds decreases with increasing Cr^{2+} doping. In addition, a broad hump (shown in the smaller inset) in the FC curve has been observed in the temperature range of 18–45 K for the compound $x = 0$. Such a broad hump in the magnetization curves has been previously reported in the literature, which is ascribed due to the presence of an antiferromagnetic short-range spin correlation between the metallic ions within the chain compounds.[54,55] The hump like structure decreases with increasing Cr^{2+} doping ($x = 0.1$) and vanishes further for the compound with $x = 0.5$. The reduction in the transition temperature and magnetization could be related to an increase in the distortion of the compound due to Cr^{2+} doping. The χT *vs.* T (χ is the *dc* magnetic susceptibility) curves at 100 Oe of $[\{Fe(\Delta)Fe(\Lambda)\}_{1-x}\{Cr(\Delta)Cr(\Lambda)\}_x(ox)_2(phen)_2]_n$ compounds for $x = 0$ and 0.1 are shown in Fig. 8(a) and (b), respectively. The χT *vs.* T curves fall slowly down to a certain temperature and after that the curves shoots up, showing a maximum value of χT and then, decreases, as the temperature is lowered further. This kind of behavior is a characteristic of ferrimagnetic materials.[11,56] Whereas, for a typical ferromagnetic compound, the χT *vs.* T curve rises continuously with the lowering of temperature, till the transition temperature is reached. Thus, the χT *vs.* T curves of both the compounds for $x = 0$ and 0.1 show characteristics of a ferrimagnetic ordering.

In addition, the temperature dependence of the inverse of the susceptibility (χ^{-1}) shown in the inset of Fig. 8, also helps to determine the nature of the magnetic ordering. In the temperature range ~70–300 K (paramagnetic region), the susceptibility can be fitted by a straight line using the Curie–Weiss law.

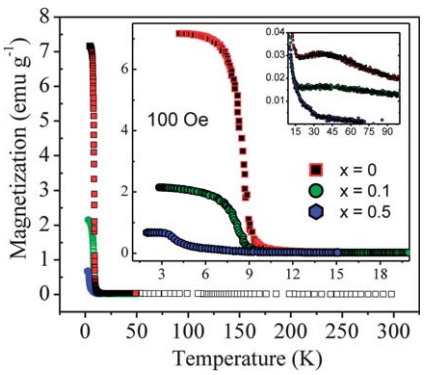

Fig. 7 The field-cooled (FC) magnetization *versus* temperature (T) curves under an external applied magnetic field of 100 Oe for the compound $[\{Fe(\Delta)Fe(\Lambda)\}_{1-x}\{Cr(\Delta)Cr(\Lambda)\}_x(ox)_2(phen)_2]_n$ with $x = 0$, 0.1, and 0.5. The bigger inset shows the magnification view of M *vs.* T curves for three different compounds, whereas the smaller inset shows a short-range spin correlation (broad hump like structure around ~40 K) for the compounds.

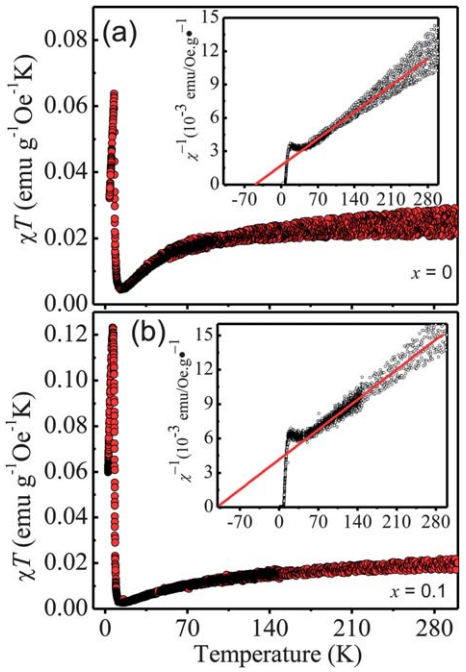

Fig. 8 χT *versus* temperature (T) curves under an external applied magnetic field of 100 Oe for the compound $[\{Fe(\Delta)Fe(\Lambda)\}_{1-x}\{Cr(\Delta)Cr(\Lambda)\}_x(ox)_2(phen)_2]_n$ with $x = 0$ (a) and 0.1 (b). The corresponding inset shows the inverse susceptibility *vs.* temperature curves fitted by using the Curie–Weiss law.

$$\chi = \frac{C}{T - \theta_p}$$

where, C is the Curie constant and θ_p is the paramagnetic Curie temperature. The values of θ_p are found to be negative and large (-49 and -110 K for the $x = 0$ and 0.1 compounds, respectively). The negative values of θ_p indicate that the interaction between both the Fe^{2+} ions {Fe(Δ) and Fe(Λ)} is antiferromagnetic in nature. The spin only effective paramagnetic moments, μ_{eff} {6.4 and 6.3 μ_B f.u.$^{-1}$ for the $x = 0$, and 0.1 compounds, respectively} are derived by using the formula $\mu_{eff} = (3Ck_B/N_A)^{1/2}\mu_B \sim (8C)^{1/2}\mu_B$, where N_A is Avogadro's number and k_B is the Boltzman constant. The theoretically expected (spin only) values of μ_{eff} are calculated by using the formula $(\mu_{eff})^2 = \Sigma[g^2\{nS(S+1)\}]\mu_B^2$, where g is gyromagnetic ratio ($\sim$2), n is the number of magnetic ions with spin S in the formula unit, and the summation Σ runs over all the magnetic ions in the formula unit. The theoretically calculated values of the spin only μ_{eff} are found to be 6.92 μ_B f.u.$^{-1}$ for all the compounds ($x = 0$, 0.1, and 0.5), assuming both the Fe^{2+} and Cr^{2+} ions are in their high spin states (*i.e.* $S = 2$ for both ions). However, for the $x = 0.1$ compound, $\sim$84% Fe^{2+} ions are in high spin state ($S = 2$), while $\sim$16% are in low spin state ($S = 0$) as obtained from the present Mössbauer study. Similarly, for the $x = 0.5$ compound $\sim$41% Fe^{2+} ions are in the high spin state, while $\sim$59% are in the low spin state. Therefore, the theoretically calculated spin only values of μ_{eff} should be, $[2^2\{1.8 \times 2 \times (2+1) \times 0.84 + 1.8 \times 0 \times (0+1) \times 0.16 + 0.2 \times 2 \times (2+1)\}^{1/2}$ $\mu_B = 6.4$ μ_B for the $x = 0.1$ and $[2^2\{1 \times 2 \times (2+1) \times 0.41 + 1 \times 0 \times (0+1) \times 0.59 + 1 \times 2 \times (2+1)\}^{1/2}$ $\mu_B = 5.8$ μ_B for the $x = 0.5$ compounds. The experimentally observed values of μ_{eff} are consistent with the theoretically calculated spin only values of compounds for $x = 0$, 0.1 and 0.5.

Furthermore, the ferrimagnetic chain nature of the compound can be viewed using the one dimensional Ising chain model, fitted to the magnetization data. In general, the ferrimagnetic chain structure shows a common characteristic feature in the magnetization data, namely a minimum at an intermediate value of kT/j, and a divergence at lower temperature, according to the power law T^{-a} ($a = 0.8$–1),[54] here k is Boltzman constant and j is coupling constant. Similar magnetic features have been obtained in chain compounds, only characterized by alternating Landé g factors. In the present case, the compound studied by employing the combined Mössbauer and XRD techniques reveals the chain structure of [-Phen-Fe(Δ)-C_2O_4-Fe(Λ)–phen–] and both the Fe^{2+} ions are different in bond lengths as well as geometrical surroundings. This suggests two different pathways of magnetic interactions and Landé g factors as follows:

…….. Fe(Δ) ———Fe(Λ)..... Fe(Δ) ———Fe(Λ).....

$j1$ ga $j2$ gb $j1$ ga $j2$

where j_1, and j_2 (coupling constants) refer to two different exchange interactions in two different pathways shown by the dotted and the solid lines, and ga, and gb are two different Landé g factors corresponding to these two interactions. The magnetization data were then fitted by using the following equation for zero field parallel susceptibility.[54]

$$\chi = \left(\frac{N\mu B^2}{2kT}\right)\frac{\{g_+^2\exp(J_+/2kT) + g_-^2\exp(-J_+/2kT)\}}{\cosh(J_-/2kT)}$$

where $g_\pm = (ga \pm gb)/2$, and $J_\pm = (j_1 \pm j_2)/2$. The fitting of magnetization data along with the influence of variation of ga, gb, j_1 and j_2 are shown in Fig. 9. The values of the parameters, and the variations of ga, gb, j_1 and j_2 suggest different possible form of chain structures. When $j_1 = j_2$ and $ga \neq gb$, the compound can be considered as a regular antiferromagnetic chain like structure, whereas when $j_1 \neq j_2$ and $ga \neq gb$, it is known as a non-regular antiferromagnetic chain. In addition, the compounds with negative j_1 and j_2 values and different Landé g factors, suggest a ferrimagnetic like nature of the compounds at low temperature. The obtained fitting parameters and the observation of local maximum (*i.e.* broad hump around $\sim$32 K, in the M *vs.* T data) confirm a non-regular antiferromagnetic 1-D chain like structure of $[\{Fe(\Delta)Fe(\Lambda)\}_{1-x}\{Cr(\Delta)Cr(\Lambda)\}_x(ox)_2(phen)_2]_n$ compound for $x = 0$. It is observed that an increasing j_1/j_2 ratio with fixed j_2 {in Fig. 9(a)} increases the broadness of a local minima which shifts towards a higher temperature range. Whereas, increasing the j_1/j_2 ratio with fixed j_1 {Fig. 9(b)}, enhances the sharpness of the local minima, and the minima shifts towards the lower temperature range. Similarly, the influence of the g value variation is shown in Fig. 9(c) and (d). For an increasing ga/gb ratio, the disappearance of the local maximum in the magnetization has occurred due to the non-zero magnetic moment, at low temperature. For the regular

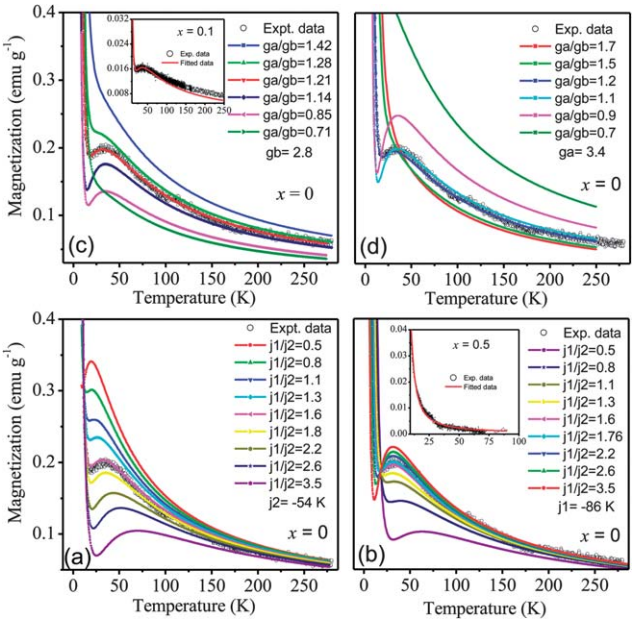

Fig. 9 (Color online) Fitting of experimental magnetization data with 1-D Ising chain model along with the theoretical variation showing the influence of the different J and g factors. (a) and (b) show variations of j_1/j_2, and variation of ga/gb (c) and (d) of the compound for $x = 0$. The insets of (c) and (b) show fitting of the compounds for $x = 0.1$ and 0.5, respectively.

chain, the maximum of the magnetization or susceptibility is conserved as long as the ratio between the Landé g factors (ga/gb) is close to unity.[54] In intermediate cases, where both j_1/j_2 and ga/gb differ from unity, one finds that the maximum of the magnetization or susceptibility is only noticeable near the dimer limit.[54] Since, the perpendicular susceptibility does not give any information regarding the nature (ferri- or antiferromagnetic) of a chain structure, we have not considered the perpendicular component of the susceptibility in the fitting in spite of the fact that the samples are polycrystalline in nature. However, it is reported[54] in the literature that, when studying powders of 1-D ferrimagnets, the main contribution in the total susceptibility (perpendicular + parallel) is mainly due to parallel component of the susceptibility. Therefore, we assume that this result also holds true for the j alternating ferrimagnetic chains as well. Thus, we conclude that the compound where $x = 0$ exhibits the typical features of 1-D ferrimagnets. A similar kind of 1-D ferrimagnetism has also been reported in bimetallic complexes characterized both by compensated and non-compensated spin sub-lattices with different g values at different (alternating) sites.[54,55,57,58] With increasing $x = 0.1$ and 0.5, the ga/gb and j_1/j_2 ratios are found to be ~1.2, 0.2 and ~2.4, 1 respectively. The fitting parameters show that the compound where $x = 0.5$ exhibits a regular antiferromagnetic chain like structure ($j_1 = j_2$ and $ga \neq gb$).

Fig. 10 shows the magnetization (M) as a function of the applied magnetic field (H) of ± 9 Tesla at different temperatures of the present compounds with $x = 0$, 0.1, and 0.5. The M *vs.* H curves for all the compounds do not show any saturation, even under an applied magnetic field of 9 Tesla. Fig. 10(a) shows M *vs.* H curve for the $x = 0$ compound at temperatures of 1.6 and 5 K. The coercivity of ~0.02 Tesla {inset of Fig. 10(a)} has been found at 5 K, however, a profound and quite large hysteresis loop is observed for the compound ($x = 0$) at 1.6 K. This means, the compound behaves as a hard magnet showing a large hysteresis loop. A giant coercive field of ~3.2 Tesla was observed in this case. The observation of a giant magnetic hysteresis, very similar to hard magnets in such type of chain magnets, is one of the remarkable phenomena observed, particularly, in the absence of a long-range magnetic ordering. The observation of larger magnetic hysteresis in zero-dimensional single molecule magnets[59] and 1-D single chain magnets[37,45] has been reported earlier, however the origin of the magnetic hysteresis is not yet well understood. For the compound with $x = 0.1$, M *vs.* H curves at three different temperatures (5, 1.9, and 1.7 K) are shown in Fig. 10(b). It has been observed that the coercive field decreases as a function of temperature, and was found to be ~0.03, 1.06, and 1.62 Tesla at 5, 1.9, and 1.7 K, respectively. Fig. 10(c) shows the M *vs.* H curves measured for the compound $x = 0.5$ at 1.7 and 5 K. The coercive fields of ~0.05 and ~0.80 Tesla have been observed at 1.7 and 5 K, respectively for the $x = 0.5$ compound. It is interesting to note that the coercive field, in contrast to all other compounds ($x = 0$, 0.1, and 0.5) increases at 5 K and decreases at ~1.7 K. In addition, the slope of the M *vs.* H curve increases with increasing Cr^{2+} doping suggesting a stronger antiferromagnetic nature of the compound. The maximum magnetization values are found to be 0.7, 0.88 and 1 μ_B f. u.$^{-1}$ for $x = 0$, 0.1 and 0.5 compounds, respectively. The theoretically expected (spin only) value of the ordered magnetic moment, μ_s per formula unit is calculated by using the formula $\mu_s = \Sigma(gnS)$ μ_B, where g is the gyromagnetic ratio (~3 obtained from the fitted magnetization data), n is the number of magnetic ions with spin S in the formula unit and the summation (Σ) runs over all the magnetic ions in the formula unit. For the $x = 0$, 0.1 and 0.5 compounds, the μ_s per formula unit (spin only) is found to be ~12 μ_B considering both Fe^{2+} and Cr^{2+} in their high spin states ($S = 2$ for both the ions). However, for the compound with $x = 0.1$, we have found from our Mössbauer study that ~84% Fe^{2+} ions are in the high spin state ($t_{2g}^4e_g^2$, $S = 2$), while ~16% are in the low spin state ($t_{2g}^6e_g^0$, $S = 0$). Therefore, the spin only ordered moment, μ_s should be $\{3 \times 1.8 \times 2 \times 0.84 + 3 \times 1.8 \times 0 \times 0.16 + 3 \times 0.2 \times 2\}$ $\mu_B = 10.2$ μ_B, for the compound with $x = 0.1$. Similarly, for the $x = 0.5$ compound, we have found from our Mössbauer study that ~41% Fe^{2+} ions are in the high spin state ($t_{2g}^4e_g^2$, $S = 2$), while ~59% are in the low spin state ($t_{2g}^6e_g^0$, $S = 0$). Therefore, the spin only ordered moment, μ_s should be $\{3 \times 1 \times 2 \times 0.41 + 3 \times 1 \times 0 \times 0.59 + 3 \times 0.2 \times 2\}$ $\mu_B = 3.6$ μ_B, for the compound with $x = 0.5$. The difference in the experimentally observed and theoretically calculated ordered moment is due to the non-saturation of the hysteresis curves even up to 9 Tesla for all the compounds. Based on the M *vs.* T and M *vs.* H results along with their loops behavior, a ferrimagnetic nature of the compound is evident. It is expected that the antiferromagnetic interactions between two Fe ions {Fe(Δ) and Fe(Λ)} in single chain magnets may exist within the chain, resulting in a ferrimagnetic ordering or a canted structure. The spin-canted structure should arise from the

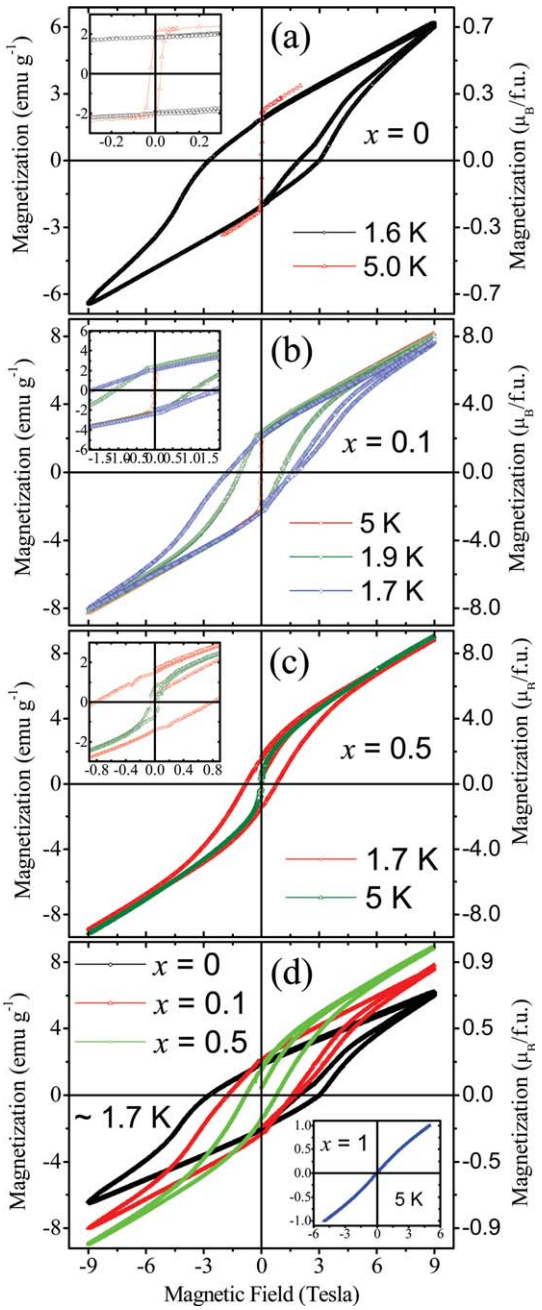

Fig. 10 Magnetization (*M*) *vs.* field (*H*) curves up to 90 KOe field for (a) $x = 0$ at 1.6 and 5 K, (b) $x = 0.1$ at 1.7, 1.9 and 5 K, (c) $x = 0.5$ at 1.7 and 5 K and (d) comparison of *M vs. H* curves for $x = 0$, 0.1 and 0.5 compounds at 1.7 K. The insets of (a), (b) and (c) show the magnified view of *M vs. H* curves for $x = 0$, 0.1 and 0.5, compounds, respectively. The inset of (d) shows *M vs. H* curve for $x = 1$ sample.

antisymmetric exchange mechanism,[60] and is consistent with the lack of an inversion center between neighboring Fe^{2+} ions within the 1-D chain.[43]

The magnetic properties can also be understood from the super exchange interaction between the Fe ions through the bridged oxalate ligands. Several parameters, such as the bond angle, bond length, doping, *etc*. determine the range of exchange interactions in the compound.[61] It is instructive to take a look at a simplified molecular orbital description of the exchange interaction in such an oxalate-bridged single chain compounds. More particularly, an initial attempt has been made to explain the exchange interaction in molecular orbital terms. In the compound ($x = 0$), both magnetic Fe^{2+} ions are at the octahedral sites within the chains with an intrachain separation of ~5 Å. On the other hand, the interchain separation (between two Fe) is of ~9 Å, and so we may neglect any possible Fe–Fe interchain coupling. Thus, the exchange coupling also known as a super exchange interaction between the Fe ions would be mediated by the oxalate ligand along the intrachain only. The possible exchange interaction between an orbital of the Fe ions through the oxalate ligand is shown in Fig. 11. Both the Fe ions {Fe(Δ) and Fe(Λ)}are in their high spin states with an electronic configuration of $t_{2g}^4e_g^2$ ($S = 2$). All electrons are arranged in their magnetic orbital t_{2g} (d_{xy}, d_{yz} and d_{zx}) and e_g (d_{z^2} and $d_{x^2-y^2}$). Since, both Fe ions have four unpaired electrons in the t_{2g} and e_g orbitals, ferromagnetic j_{FM} as well as antiferromagnetic j_{AFM} interactions are possible between the Fe ions through the oxalate ligand. Thus, the coupling constant (J) can be decomposed into two terms, one ferromagnetic j_{FM} and other antiferromagnetic j_{AFM} as per the following equation:

$$J = j_{FM} + j_{AFM}$$

When $j_{FM} > j_{AFM}$, the dominant interaction will be ferromagnetic, and if $j_{FM} < j_{AFM}$ the dominant interaction will be antiferromagnetic in nature. However, the exchange constant for a ferromagnetic coupling between the Fe ions arises due to an orthogonality of their magnetic orbitals *i.e.* the super exchange interaction is ferromagnetic (FM) only with ions of different orbital symmetries.[62] While the exchange constant for an antiferromagnetic coupling arises due to a non-orthogonality (overlap) of their magnetic orbitals *i.e.* the super exchange interaction is antiferromagnetic (AFM) only with ions of similar orbital symmetries.[62] In addition, since the oxalate ligand possesses four different orbital symmetric {two symmetric ($^1z^2$ and $^1xy)_S$ and two asymmetric ($^1z^2$ and $^1xy)_A$} as labeled in Fig. 11(a), the exchange interaction depends upon the interactions between the two Fe(II) d orbitals through an appropriate symmetry of molecular orbitals of the bridging group. It is these four lone-pair orbitals that provide the greatest interaction with the prescribed combinations of d orbitals and lead to an energy difference between a pair of symmetric and anti-symmetric orbitals.[61] Now, let us consider the case of an exchange interaction of two d_{z^2} orbitals of Fe ions through a $(^1z^2)_S$ orbital of the oxalate ligand in the compound. Fig. 11(b) presents an exchange interaction scheme between two d_{z^2} orbitals of Fe ions through the $(^1z^2)_S$ orbital of the oxalate, considering the crystallographic geometry of the chain structure. It is clear from the scheme that d_{z^2} orbital of the Fe_1{Fe(Δ)} ion is parallel to the π orbital of one of the oxygen atoms of the oxalate ligand and perpendicular to the other oxygen atoms. In addition, the d orbitals of the Fe ions are confined to the plane of the oxalate ligand. This means that the d_{z^2} orbital of the Fe_1 ion and the π orbital of the oxalate are orthogonal (perpendicular) to each

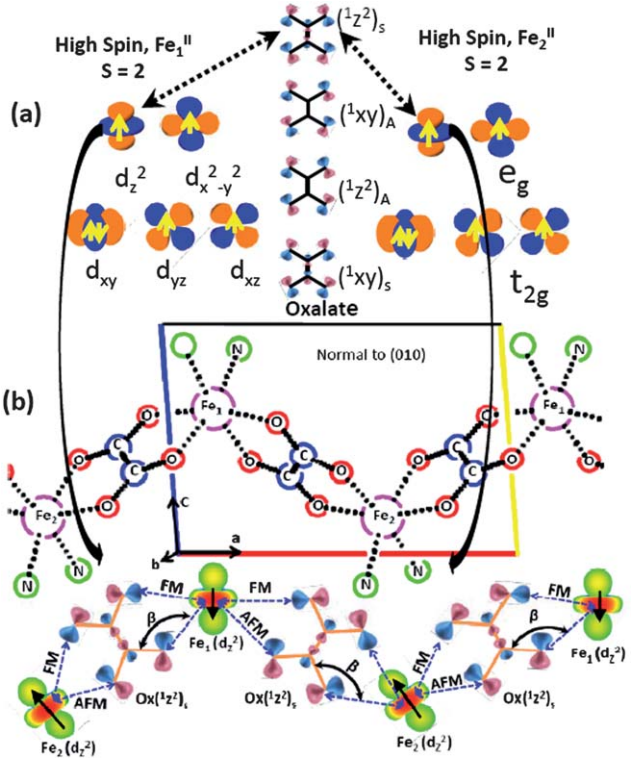

Fig. 11 (a) Schematic diagram of the magnetic exchange interaction between the Fe_1 and Fe_2 ions through the oxalate ligand. The possible electron transfers between the orbitals (e_g, t_{2g} of the Fe^{2+} ions and the $^1z^2$, ^1xy of the oxalate ligand) are shown by the dotted lines. (b) Magnetic exchange interaction scheme to view the super exchange pathways (blue color dotted line) between the d_{z^2} orbitals of the Fe through the oxalate ligand in the compound (shown crystallographically along the unit cell). The large and small arrows (black) correspond to the ordered magnetic moments.

other and yield a ferromagnetic interaction, whereas the parallel arrangement would provide the antiferromagnetic interaction in the compound due to the non-orthogonality of their orbitals. However, it is known from our XRD study that the Fe_2 {Fe(Λ)} ions have a lower bond length and bond angle with the oxygen atoms of the oxalate ligand compared to those for the Fe_1 {Fe(Δ) ion along the intrachain. *i.e.* the oxalate structure is considerably distorted from the octahedral symmetry with respect to each other with significant lengthening of one of the Fe–O bonds. These atomic arrangements provide a more favorable parallel (non orthogonal) overlap between the d_{z^2} orbital of the Fe_2 and the π orbital of the oxalate, resulting in a strong antiferromagnetic interaction as compared to the ferromagnetic interaction. Thus, both ferromagnetic and antiferromagnetic super exchange interactions (*via* oxalate ligand) coexist between the Fe ions and compete with each other resulting in a net ferrimagnetic nature of the compound. With increasing Cr^{2+} doping, it is evident from the XRD and crystal structure shown in Fig. 3, that the bond length and bond angles between both Fe ions are decreasing *i.e.* in the present scenario, the ferromagnetic exchange pathway distance between the d_{z2} orbital of Fe_1 ion and the π orbital of the oxalate is decreasing. This means that the contribution from the net ferromagnetic interaction is decreasing and simultaneously on the other side, the contribution from the antiferromagnetic interaction increases in the compound. Thus, with increasing Cr^{2+} doping the compound tends towards a perfect antiferromagnetic type (for $x = 0.5$). Our theoretically fitted parameters (j_1,j_2) using the 1-D Ising chain model of magnetization also suggest that the compound tends towards a more antiferromagnetic type with Cr^{2+} doping.

(D) *ac* susceptibility and magnetic relaxation study

In order to obtain further information on the magnetically ordered regime, *ac* magnetic susceptibility measurements at different frequencies were performed for the compounds $x = 0$ {Fig. 12(a)} and $x = 0.1$ {Fig. 12(b)} in a zero applied static field with an oscillating field of 5 Oe. It shows a peak maxima, both in the in-phase (χ'), and the out-of-phase (χ''), magnetic susceptibilities, which is frequency dependent. The peak temperature is known as the transition temperature (T_P) and is found to be ~8.7 K at a low frequency of 48.7 Hz for both the in-phase and out-of-phase curves. In addition, it is observed that the peak position increases and the amplitude decreases slightly with increasing frequency. The T_P is found to be ~8.9 K at a frequency of 987 Hz. A similar behavior has been found for the $x = 0.1$ compound. This frequency dependent *ac* susceptibility behavior indicates a cooperative freezing of individual magnetic moments, characteristic of spin-glasses,[63–66] superparamagnets[67] or SCMs.[68,69] However, it has been shown earlier that both the in-phase (χ') and out-of-phase (χ'') components are frequency dependent and their peak maxima shifted to lower temperatures as the *ac* frequency was lowered, indicating a slow relaxation of the magnetization and is characteristic of a SCM.[70]

The most commonly used experimental measure of a "relaxation time" τ, which describes the dynamical fluctuation time scale, is obtained from the observation time t. This is due to the fact that the characteristic relaxation time of the system at the in-phase susceptibility maximum corresponds to the observation time $t = 1/f$. The frequency dependence of the *ac* susceptibility was studied by the equation $\Psi = \Delta T_P/[T_P \times \Delta(\log_{10} f)]$, where ΔT_P is the difference between T_P measured in the $\Delta\log_{10} f$ frequency interval. The estimated value of Ψ for the compound $x = 0$ is 0.02, which is close to a normal value for spin glass (0.01–0.08).[45,66] However, the relaxation time τ has been determined form the maximum of the susceptibility curve at a given temperature according to Glauber's theory[71] using the Arrhenius law:

$$\tau(T) = \tau_0 \exp\left(\frac{\Delta}{k_B T}\right) \quad (1)$$

where, τ is the relaxation time, τ_0 is the pre-exponential factor, and Δ is the energy barrier. At $T = T_P$, the above eqn (1) can be rewritten as:

$$\frac{1}{T_P} = -\frac{k_B}{\Delta}\{\ln(2\pi f) + \ln(\tau_0)\} \quad (2)$$

We have plotted $1/T_P$ *versus* $\ln(2\pi f)$ in Fig. 13(a). The experimental data follow a linear variation, which confirms the

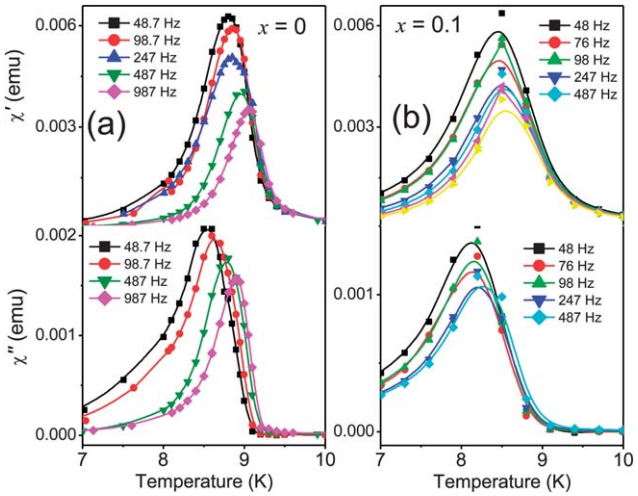

Fig. 12 The temperature dependence of the in-phase (χ') and of out-of-phase (χ'') magnetic *ac* susceptibility recorded at various frequencies for the $x = 0$ (a) and $x = 0.1$ (b) compounds. The oscillating field of 5 Oe was used for all the measurements.

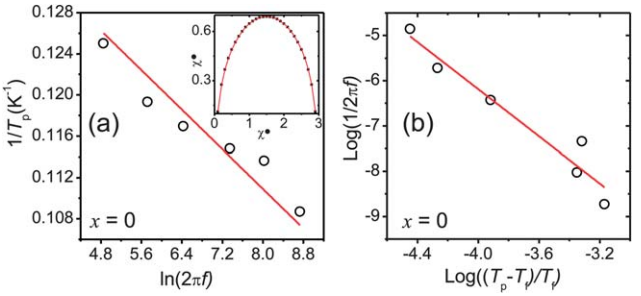

Fig. 13 $1/T_P$ *versus* $\ln(2\pi f)$ plot for the compound $x = 0$ (a) the solid line denotes the least-squares fitting of χ'' to the Arrhenius equation. The inset shows a Cole–Cole diagram obtained using a Debye model. (b) log–log plot of the reciprocal of the frequency ($\tau = 1/f$) *vs.* ($T_P/T_f - 1$). The solid line is the fitted curve using the power law.

theoretical predictions. The fitted parameters are found to be $\Delta/k_B = 208$ K and $\tau_0 = 2.9 \times 10^{-14}$ s indicates higher value of energy barrier. However, higher value of energy barrier (~350 K) has been previously reported for the ferromagnetic spin chain magnet as well.[45] The large energy barrier is expected due to the linkage of oxalate ligand with metallic ions and could be originated from the magnetic anisotropy of the compound. The obtained parameter matches with the previously reported values for spin chain magnets.[37,45,72] In addition, at a fixed temperature, we obtain a semicircle Cole–Cole diagram {inset of Fig. 13(a)}, as expected for a Debye model[73] with a single relaxation time.[37] In order to get a better idea of the low temperature magnetic behavior, the frequency dependence of T_P has been fitted by a power law. The power law assumes the existence of a true equilibrium phase transition at the freezing temperature T_g and described as

$$\tau(T_P) = \tau_0\left(\frac{T_P}{T_g} - 1\right)^{-zv} \quad (3)$$

where, τ_0 is related to the relaxation of the individual cluster magnetic moment and $zv$is a critical exponent. The log–log plot shown in Fig. 13(b) shows the fitting of the T_P using power law for the $x = 0$ compound. In this case, the best linear fit has been achieved with $T_g = 8.55$ K, $\tau_0 = 6.1 \times 10^{-8}$ s, and $zv = 2.6$. It is observed that the obtained value of $-zv$ is out of the range (from 4 to 12) for various spin glasses, therefore ruling out the possibility of having a spin glass nature of the compound.[66,74] A similar value of $zv = 3.3$ has also been previously observed for a ferrimagnetic chain based on cobalt hydroxysulfate compounds.[72] Therefore, from the *ac* susceptibility study we conclude that the compound follows Glauber dynamics and behaves like a single-chain magnet.

The observation of single-chain magnetic behavior can also be directly confirmed by using a magnetization relaxation measurement. Fig. 14 shows the field cooled magnetization *vs.* time (t) measurements at 1.5 K for the compounds where $x = 0$ and $x = 0.1$. The compounds were first cooled down to 1.5 K from room temperature in a zero field, then a 5 Tesla magnetic field was applied for a period of 10 s, and subsequently M was recorded as a function of time by removing the field. Both compounds show the relaxation effect, however, the relaxation is found to be slow for the compound where $x = 0$ compared to $x = 0.1$ suggesting the low dimensional nature of the compound. The experimental data were fitted using the exponential decay equation, $y = y_0 + A\exp^{-x/t}$ where t is the decay constant. The decay constants of ~9781 and 1326 s have been found for the compounds $x = 0$ and $x = 0.1$, respectively. Therefore, the observation of a slow relaxation on the macroscopic time scale for the compound $x = 0$ confirms that the compound is a 1-D single-chain magnet.[75,76]

(E) High pressure magnetization study

The effect of hydrostatic pressure on the magnetic property has been determined for the compound where $x = 0$. The field-cooled (FC) magnetization *versus* temperature (T) curves under an external applied magnetic field of 100 Oe are shown in Fig. 15(a) as a function of pressure up to 0.8 GPa. The transition temperature (T_C) is found to ~9.2 K at ambient pressure.

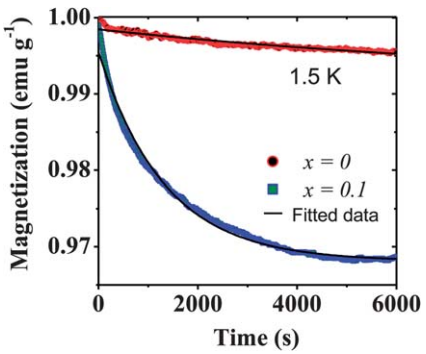

Fig. 14 Normalized magnetization (M) *vs.* time curves showing the relaxation effect at 1.5 K for the compounds where $x = 0$ and 0.1. The black solid line represents the best fit of the experimental data using an exponential equation (see the text).

However, the enhancement in the transition temperature is clearly evident with increasing pressure {Fig. 15(b)}. The transition temperature, at a pressure of 0.8 GPa is found to be ~10.8 K indicating that the nature of the compound is tending towards antiferromagnetic with increasing pressure. The enhancement in transition temperature with pressure can be understood from the nature of the magnetic interaction between the chains (interchain and intrachain magnetic interactions) in such one-dimensional molecular magnets using the formula:[77]

$$T_C = 2S(S+1)\sqrt{4 j_{intra}\, j_{inter}} \quad (4)$$

where, T_C is the transition temperature. It can be shown from the above formula that the weak interchain interactions j_{inter} in the presence of a strong intrachain coupling j_{intra} can give rise to a finite critical temperature T_C.[77] At the ambient pressure (0 GPa), there is no interaction between the interchains. It is also clear from the XRD study that there are no chemical bonds between the interchains and the interchain distance is also very large (~9 Å). Therefore, only intrachain interactions are present in the compound without interchain interactions at ambient pressure. However, with an increasing hydrostatic pressure, the compressibility in directions perpendicular to the chains would be expected to be much larger than along the chains. Thus, with an increasing pressure, along with the intrachain interaction, the interchain interaction (which mainly depends on the pressure-induced changes in the Fe–Fe distance between interchains) will also dominate. Moreover, the π–π interactions between the two phenanthroline ligand along the intra- and interchain may also contribute in the interaction due to increasing pressure. Since, the intrachains are ferrimagnetic in nature, the combinations of such ferrimagnetic chains may lead to ferromagnetic or antiferromagnetic interchain interactions in the compound resulting in a dipolar type interaction between the intrachains. Hence, the dipolar type interaction increases the transition temperatures of the compounds. However, in quasi 1-D systems, the conditions for the appearance of ferromagnetism originating from dipolar interchain interactions are less obvious.[77] In addition, if the dipolar interactions between the chains are the sole interchain interaction, then from eqn (4), one would expect T_C to increase with the applied pressure, according to $T_C \propto d^{-3/2}$.[77] However, this is not true in the present study, therefore we can conclude that the π–π interactions between the two phenanthroline ligand are also contributing, apart from the interchain interactions with an application of hydraulic pressure.

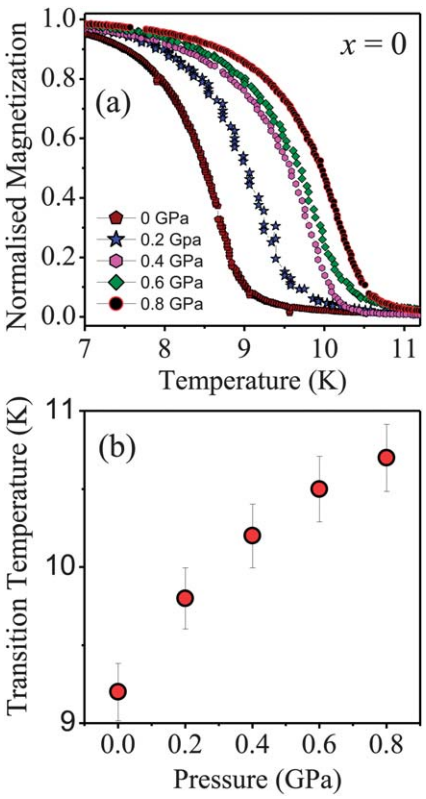

Fig. 15 (a) Normalized magnetization (*M*) *vs.* temperature (*T*) curves at different pressures and (b) variation of the transition temperature as a function of pressure for the compound $x = 0$.

Conclusion

We report the synthesis of an oxalate and phenanthroline based 1-D spin chain molecule magnet using a hydrothermal method in this paper. The detailed structural and magnetic properties of the 1-D chain like structure have been characterized using X-ray and neutron diffraction techniques, Mössbauer spectroscopy, *dc* magnetization measurements (with or without high pressure) and *ac* susceptibility. The compound exhibits new fascinating magnetic behaviors similar to the one predicted by Glauber for Ising-type chains along with a ferrimagnetic nature of the intrachains due to alternatingly spaced magnetic Fe sites. The frequency dependent *ac* susceptibility excludes the possibility of spin glass behavior and confirms that the compound is a real ferrimagnetic one-dimensional single chain magnet. The proposed super exchange interaction pathways reveal that both ferromagnetic and antiferromagnetic interactions (*via* the oxalate ligand) coexist between the Fe ions, which compete with each other, thus resulting in a net ferrimagnetic nature of the intrachain. An important characteristic of our system is the observation of spontaneous magnetization below 9 K and a giant coercivity of 3.2 Tesla in such 1-D chain magnets. In addition, it is remarkable to see an enhancement in the transition temperature in high pressure dependent magnetization measurements. This work opens new perspectives for designing new low dimensional chain magnets with giant coercivity using appropriate choice of ligands in a hydrothermal synthesis method.

Acknowledgements

The authors would like to thank Dr A. Das for help in the neutron diffraction measurements.

References

1 O. Kahn, *Molecular Magnetism*, VCH, New York, 1993.
2 J. Mroziński, *Coord. Chem. Rev.*, 2005, **249**, 2534–2548.
3 S. J. Blundell and F. L. Pratt, *J. Phys.: Condens. Matter*, 2004, **16**, R771.
4 R. G. Hicks, *Nat. Chem.*, 2011, **3**, 189–191.
5 S. K. Pal, P. Bag, A. Sarkar, X. Chi, M. E. Itkis, F. S. Tham, B. Donnadieu and R. C. Haddon, *J. Am. Chem. Soc.*, 2010, **132**, 17258–17264.
6 L. Bogani and W. Wernsdorfer, *Nat. Mater.*, 2008, **7**, 179–186.
7 M. Urdampilleta, S. Klyatskaya, J.-P. Cleuziou, M. Ruben and W. Wernsdorfer, *Nat. Mater.*, 2011, **10**, 502–506.
8 B. G. Morin, C. Hahm, J. S. Miller and A. J. Epstein, *J. Appl. Phys.*, 1994, **75**, 5782–5784.
9 E. Coronado, P. Delhaes, D. Gatteschi and J. S. Miller, *Molecular Magnetism: From Molecular Assemblies to the Device*, NATO ASI Series, Washington DC, 1995.
10 P. Bhatt, S. M. Yusuf, M. D. Mukadam and J. V. Yakhmi, *J. Appl. Phys.*, 2010, **108**, 023916.
11 P. Bhatt, N. Thakur, M. D. Mukadam, S. S. Meena and S. M. Yusuf, *J. Phys. Chem. C*, 2013, **117**, 2676.
12 A. Kumar, S. M. Yusuf, L. Keller and J. V. Yakhmi, *Phys. Rev. Lett.*, 2008, **101**, 207206.
13 P. Bhatt, A. Kanciurzewska, E. Carlegrim, M. Kapilashrami, L. Belova, K. V. Rao and M. Fahlman, *J. Mater. Chem.*, 2009, **19**, 6610.
14 P. Bhatt, S. M. Yusuf, R. Bhatt and G. Schütz, *Appl. Phys. A: Mater. Sci. Process.*, 2012, **109**, 459–469.
15 Z. J. Zhong, N. Matsumoto, H. Okawa and S. Kida, *Chem. Lett.*, 1990, 87.
16 H. Oshio and U. Nagashima, *Inorg. Chem.*, 1992, **31**, 3295–3301.
17 S. Decurtins, H. W. Schmalle, H. R. Ostwald, A. Linden, J. Ensling, P. Gütlich and A. Hauser, *Inorg. Chim. Acta*, 1994, **216**, 65–73.
18 S. Decurtins, H. W. Schmalle, P. Schneuwly and H. R. Ostwald, *Inorg. Chem.*, 1993, **32**, 1888–1892.
19 G.-F. Xu, Q.-L. Wang, P. Gamez, Y. Ma, R. Clérac, J. Tang, S.-P. Yan, P. Cheng and D.-Z. Liao, *Chem. Commun.*, 2010, **46**, 1506–1508.
20 E. Coronado, J. R. Galan-Mascaros, C. J. Gomez-Garcıa and C. MartıGastaldo, *Inorg. Chem.*, 2005, **44**, 6197–6202.
21 E. Coronado, J. R. Galán-Mascarós and C. Martí-Gastaldo, *J. Am. Chem. Soc.*, 2008, **130**, 14987–14989.
22 J. R. Galán-Mascarós, E. Coronado, P. A. Goddard, J. Singleton, A. I. Coldea, J. D. Wallis, S. J. Coles and A. Alberola, *J. Am. Chem. Soc.*, 2010, **132**, 9271–9273.
23 E. Coronado, C. Martí-Gastaldo, J. R. Galán-Mascarós and M. Cavallini, *J. Am. Chem. Soc.*, 2010, **132**, 5456–5468.
24 H. Tamaki, Z. J. Zhong, N. Matsumoto, S. Kida, M. Koikawa, N. Achiwa, Y. Hashimoto and H. Okawa, *J. Am. Chem. Soc.*, 1992, **114**, 6974.
25 E. Coronado, J. R. Galán-Mascarós, C. J. Gómez-García and J. M. Martínez-Agudo, *Adv. Mater.*, 1999, **11**, 558–561.
26 C. Mathonière, S. G. Carling, D. Yusheng and P. Day, *J. Chem. Soc., Chem. Commun.*, 1994, 1551.
27 F. Pointillart, C. Train, M. Gruselle, F. Villain, H. W. Schmalle, D. Talbot, P. Gredin, S. Decurtins and M. Verdaguer, *Chem. Mater.*, 2004, **16**, 832–841.
28 E. Coronado, J. R. Galán-Mascarós, C. J. Gómez-García and V. Laukhin, *Nature*, 2000, **408**, 447–449.
29 E. Coronado, J. R. Galan-Mascaros and C. M. Gastaldo, *J. Mater. Chem.*, 2006, **16**, 2685–2689.
30 J. B. Goodenough, *Magnetism and the chemical bond*, Interscience, New York, 1963.
31 E. Coronado, C. Martí-Gastaldo, E. Navarro-Moratalla, A. Riberaab and J. R. Galán-Mascarósc, *J. Mater. Chem.*, 2010, **20**, 9476–9483.
32 D. J. Price, A. K. Powell and P. T. Wood, *Dalton Trans.*, 2003, 2478–2482.
33 A. Caneschi, D. Gatteschi, N. Lalioti, C. Sangregorio, R. Sessoli, G. Venturi, A. Vindigni, A. Rettori, M. G. Pini and M. A. Novak, *Angew. Chem., Int. Ed.*, 2001, **40**, 1760–1763.
34 L. M. Toma, R. Lescouëzec, J. Pasán, C. Ruiz-Pérez, J. Vaissermann, J. Cano, R. Carrasco, W. Wernsdorfer, F. Lloret and M. Julve, *J. Am. Chem. Soc.*, 2006, **128**, 4842–4853.
35 H. Miyasaka, R. Clérac, K. Mizushima, K.-i. Sugiura, M. Yamashita, W. Wernsdorfer and C. Coulon, *Inorg. Chem.*, 2003, **42**, 8203–8213.
36 M. Ferbinteanu, H. Miyasaka, W. Wernsdorfer, K. Nakata, K.-i. Sugiura, M. Yamashita, C. Coulon and R. Clérac, *J. Am. Chem. Soc.*, 2005, **127**, 3090–3099.
37 R. Clérac, H. Miyasaka, M. Yamashita and C. Coulon, *J. Am. Chem. Soc.*, 2002, **124**, 12837–12844.
38 H.-L. Sun, Z.-M. Wang and S. Gao, *Coord. Chem. Rev.*, 2010, **254**, 1081.
39 L. Bogani, A. Vindigni, R. Sessoli and D. Gatteschi, *J. Mater. Chem.*, 2008, **18**, 4750.
40 L.-W. Huang, C.-J. Yang and K.-J. Lin, *Chem.–Eur. J.*, 2002, **8**, 396–400.
41 V. Russell, D. Craig, M. Scudder and I. Dance, *CrystEngComm*, 2001, **3**, 96–106.
42 J. Kim, U. Lee and B. K. Koo, *Bull. Korean Chem. Soc.*, 2010, **31**, 487–490.
43 L.-L. Li, K.-J. Lin, C.-J. Ho, C.-P. Sun and H.-D. Yang, *Chem. Commun.*, 2006, 1286–1288.
44 S. Giri and S. K. Saha, *J. Phys. Chem. Lett.*, 2011, **2**, 1567–1571.
45 N. Ishii, Y. Okamura, S. Chiba, T. Nogami and T. Ishida, *J. Am. Chem. Soc.*, 2008, **130**, 24–25.
46 D. Maspoch, L. Catala, P. Gerbier, D. Ruiz-Molina, J. Vidal-Gancedo, K. Wurst, C. Rovira and J. Veciana, *Chem.–Eur. J.*, 2002, **8**, 3635–3645.
47 T. Roisnel and J. Rodriguez-Carvajal, WINPLOTR: A Windows tool for powder diffraction patterns analysis, *Materials Science Forum*, 2000, 118–123.
48 K.-A. Wilhelmi, *Acta Chem. Scand.*, 1968, **22**, 2565–2573.
49 N. N. Greenwood and T. C. Gibb, *Mössbauer Spectroscopy*, Chapman and Hall Ltd., London, 1971.
50 S. S. Shinde, S. S. Meena, S. M. Yusuf and K. Y. Rajpure, *J. Phys. Chem. C*, 2011, **115**, 3731.
51 S. R. Naik, A. V. Salker, S. M. Yusuf and S. S. Meena, *J. Alloys Compd.*, 2013, **566**, 54–61.

52 A. Kumar, S. M. Yusuf, L. Keller, J. V. Yakhmi, J. K. Srivastava and P. L. Paulose, *Phys. Rev. B: Condens. Matter Mater. Phys.*, 2007, **75**, 224419.
53 A. Kumar, S. M. Yusuf and L. Keller, *Phys. Rev. B: Condens. Matter Mater. Phys.*, 2005, **71**, 054414.
54 E. Coronado, M. Drillon, P. R. Nugteren, L. J. d. Jongh and D. Beltrane, *J. Am. Chem. Soc.*, 1988, **110**, 3907–3913.
55 C. J. Ho, J. L. Her, C. P. Sun, C. C. Yang, C. L. Huang, C. C. Chou, L.-L. Li, K. J. Lin, W. H. Li, J. W. Lynn and H. D. Yang, *Phys. Rev. B: Condens. Matter Mater. Phys.*, 2007, **76**, 224417.
56 N. Thakur, S. M. Yusuf and J. V. Yakhmi, *Phys. Chem. Chem. Phys.*, 2010, **12**, 12208.
57 E. Coronado, l. M. Drillon, A. Fuertes, D. Beltran, A. Mosset and J. Galy, *J. Am. Chem. Soc.*, 1986, **108**, 900–905.
58 P. Román, C. Guzmán-Miralles, A. Luque, J. I. Beitia, J. Cano, F. Lloret, M. Julve and S. Alvarez, *Inorg. Chem.*, 1996, **35**, 3741–3751.
59 R. Sessoli, H. L. Tsai, A. R. Schake, S. Wang, J. B. Vincent, K. Folting, D. Gatteschi, G. Christou and D. N. Hendrickson, *J. Am. Chem. Soc.*, 1993, **115**, 1804.
60 S. J. Rettig, A. Storr, D. A. Summers, R. C. Thompson and J. Trotter, *J. Am. Chem. Soc.*, 1997, **119**, 8675–8680.
61 T. R. Felthouse, E. J. Laskowski and D. N. Hendrickson, *Inorg. Chem.*, 1977, **16**, 1077–1089.
62 M. Verdaguer, *Polyhedron*, 2001, **20**, 1115–1128.
63 M. Ferbinteanu, H. Miyasaka, W. Wernsdorfer, K. Nakata, K. Sugiura, M. Yamashita, C. Coulon and R. Clérac, *J. Am. Chem. Soc.*, 2005, **127**, 3090.
64 R. V. Chamberlin, M. Hardiman, L. A. Turkevich and R. Orbach, *Phys. Rev. B: Condens. Matter Mater. Phys.*, 1982, **25**, 6720.
65 M. D. Mukadam, A. Kumar, S. M. Yusuf, J. V. Yakhmi, R. Tewari and G. K. Dey, *J. Appl. Phys.*, 2008, **103**, 123902–123907.
66 J. A. Mydosh, *Spin Glasses: An Experimental Introduction*, Taylor & Francis, London, 1993.
67 K. Bernot, L. Bogani, A. Caneschi, D. Gatteschi and R. Sessoli, *J. Am. Chem. Soc.*, 2006, **128**, 7947.
68 A. V. Palii, O. S. Reu, S. M. Ostrovsky, S. I. Klokishner, B. S. Tsukerblat, Z.-M. Sun, J.-G. Mao, A. V. Prosvirin, H.-H. Zhao and K. R. Dunbar, *J. Am. Chem. Soc.*, 2008, **130**, 14729.
69 K. Bernot, J. Luzon, R. Sessoli, A. Vindigni, J. Thion, S. Richeter, D. Leclercq, J. Larionova and A. v. d. Lee, *J. Am. Chem. Soc.*, 2008, **130**, 1619.
70 W.-X. Zhang, T. Shiga, H. Miyasaka and M. Yamashita, *J. Am. Chem. Soc.*, 2012, **134**, 6908–6911.
71 R. J. Glauber, *J. Math. Phys.*, 1963, **4**, 294.
72 X.-M. Zhang, C.-R. Li, X.-H. Zhang, W.-X. Zhang and X.-M. Chen, *Chem. Mater.*, 2008, **20**, 2298–2305.
73 K. S. Cole and R. H. Cole, *J. Chem. Phys.*, 1941, **9**, 341.
74 T.-F. Liu, D. Fu, S. Gao, Y.-Z. Zhang, H.-L. Sun, G. Su and Y.-J. Liu, *J. Am. Chem. Soc.*, 2003, **125**, 13976–13977.
75 H. Miyasaka, M. Julve, M. Yamashita and R. Clerac, *Inorg. Chem.*, 2009, **48**, 3420.
76 D. Gatteschi and A. Vindigni, arXiv:1303.3731, 2013.
77 F. Mascarenhas, K. Falk, P. Klavins, J. S. Schilling, Z. Tomkowicz and W. Haase, *J. Magn. Magn. Mater.*, 2001, **231**, 172–178.

